

# Entanglement Structures in Quantum Field Theories: Negativity Cores and Bound Entanglement in the Vacuum

Natalie Klco,<sup>1,\*</sup> D. H. Beck,<sup>2,†</sup> and Martin J. Savage<sup>3,‡</sup>

<sup>1</sup>*Institute for Quantum Information and Matter and Walter Burke Institute for Theoretical Physics,  
California Institute of Technology, Pasadena CA 91125, USA*

<sup>2</sup>*Department of Physics and Illinois Quantum Information Science and Technology (IQUIST) Center,  
University of Illinois at Urbana-Champaign, Urbana, IL 61801, USA*

<sup>3</sup>*InQuBator for Quantum Simulation (IQuS), Department of Physics,  
University of Washington, Seattle, WA 98195, USA*

(Dated: February 10, 2022 - 2:21)

A deep understanding of quantum field theory entanglement structure is valuable for designing and performing efficient quantum simulations beyond the capabilities of classical computation. In the covariance matrix formalism for Gaussian continuous variables, we present the first evidence of bound entanglement between disjoint regions of the vacuum in one-dimensional non-interacting scalar field theory. This inaccessible entanglement is found to mirror the distillable entanglement, both in magnitude and its exponential envelope, but with a striking step behavior. To reveal the entanglement structure, we develop new techniques, including a local unitary that transforms the many-body entanglement of the field into a tensor-product *core* of  $(1 \times 1)_{\text{mixed}}$  pairs and a *halo* that is separable when isolated from the core but contains underlying, separability-obscured entanglement (SOE). These features are expected to persist in higher dimensions and in more complex theories relevant to Standard Model physics, and may provide a language for describing the dynamics of information in quantum chromodynamics as quarks and gluons transition to hadrons through the confinement and chiral symmetry breaking scales.

As experimental control and manipulation of quantum many-body (QMB) systems become more precise, theoretical advances in the fundamental understanding of entanglement continue to uncover intriguing relations and classifications of quantum information structures and dynamics. Considering quantum correlations as a valuable resource for tasks of computation and simulation [1] has begun to provide unique insights [2–18] and capabilities to robustly explore physical systems from the Standard Model and its quantum field theories (QFTs) [19–22] to gravitation. Conversely, because quantum fields naturally distribute entanglement dynamically and at spacelike separations [23–30], their quantum correlations have long been recognized as a resource in quantum information protocols, e.g., sensing, communications, simulations, and computing. Bringing these potential applications to fruition necessitates detailed and operational understanding of the quantum correlation structures within the field and its representation(s) on quantum devices.

Following decades of remarkable progress in unraveling the entanglement structures of QFTs [31–53], leveraging both analytic techniques including the AdS/CFT correspondence and numerical techniques of lattice field theory and harmonic chains, substantial experimental efforts have begun to quantify entanglement structures in low-dimensional QFTs, e.g., Refs. [54–56]. However, many quantum correlation properties that may guide simulation protocols, e.g., for scalar fields [57–71] towards gauge field theories [72–117], require further study.

In this work, we determine the following properties of the entanglement distributed between two disjoint regions of the free scalar field vacuum:

- The distillable entanglement saturates the upper bound set by the negativity measure.
- Inaccessible bound entanglement is also present and mirrors the distillable entanglement.

First, we extend the physical significance of negativity [118–121]. For generic Gaussian states, a calculation of non-zero negativity provides an upper bound, as well as a lower bound excluding zero [122], to the entanglement that may be distilled from a bipartite system. For the free scalar field, the saturation of this value promotes the negativity from an upper bound to a quantity with direct physical and operational meaning. Second, quantifying the bound entanglement [123–129] reveals it to be commensurate in magnitude with the distillable entanglement and to exhibit intriguing plateaus as the continuum is approached. While not available as an experimental quantum resource, the presence of this entanglement structure is likely to impact experimental state preparation and quantum simulation design.

To determine these features of scalar field entanglement, we develop a constructive methodology for calculating local unitary operations that concentrate the entirety of the distillable entanglement into a subset of *core* modes. We show the remaining modes form a separable *halo* with entanglement that is obscured by classical correlations. This provides a concrete demonstration uncoupling the relationship between separability and vanishing entanglement: subsystems of mixed states that are classically connected to the whole may be separable in isolation but still require underlying entanglement in context of the larger QMB system. This structure of non-simultaneous separability among the transformed field regions has been leveraged as a protocol for revealing previously unidentifiable bound entanglement.

\* [natklco@caltech.edu](mailto:natklco@caltech.edu)

† [dhbeck@illinois.edu](mailto:dhbeck@illinois.edu)

‡ [mjs5@uw.edu](mailto:mjs5@uw.edu); On leave from the Institute for Nuclear Theory.

Beyond identification, these methods offer new capabilities to quantify bound entanglement and clarify physical mechanisms that lead entanglement to become bound or, more broadly, obscured when a system or subsystem satisfies the separability criterion.

**Transformations to a Core and Halo** Extracting a pair of regions from the vacuum of a lattice scalar field theory generates a class of  $(d \times d)_{\text{mixed}}$  continuous variable (CV) states parameterized by the region pixelation  $d$ , their separation  $\tilde{r}$ , and the mass  $m$  of the field <sup>1</sup>. For free fields with quadratic Hamiltonians, the field is represented by the Gaussian subset of CV states [130, §S1], where density matrix entanglement properties are characterized by associated covariance matrices (CMs) with matrix elements analytically defined by the set of two-point correlation functions,  $G = \langle \phi_i \phi_j \rangle$  and  $H = \langle \pi_i \pi_j \rangle$ . Symplectic transformations of the CMs correspond to unitary operations in the Hilbert space that automatically incorporate the commutation relations of the field.

Although a number of entanglement structure reorganizations have been devised for CV systems [35, 122, 127, 131–137], the transformation developed here [130, §S2] achieves clear separation of the distillable and bound entanglement. This is depicted in Fig. 1, where the  $A$  and  $B$  spaces label the two regions of the vacuum. Our restructuring of the CM is achieved through *local* symplectic transformations that are calculated from a subset of the symplectic eigenvectors of the full, partially transposed (PT) CM (or product  $GH$ ). The subset corresponds to the  $d$  lowest PT symplectic eigenvalues, where  $n_-$  of the eigenvalues contribute to the negativity with  $n_- \leq d$ . Within this subset, components corresponding to a single region are extracted, and the phase space structure is repaired using a Gram-Schmidt orthogonalization process modified to incorporate symplectic inner products. The resulting symplectic operations are applied locally to each region,

$$\sigma' = (S_A \oplus S_B) \sigma (S_A \oplus S_B)^T, \quad (1)$$

transitioning between the original CM  $\sigma$ , the fully entangled modes of the vacuum regions, and  $\sigma'$ , an organized core of  $n_c = n_-$  entangled  $(1 \times 1)_{\text{mixed}}$  states containing the distillable entanglement and a halo space with separability-obscured entanglement (SOE).

**Separability-Obscured Entanglement** For Gaussian states, separable mixed-state CMs may be generically decomposed as  $\sigma_{\text{sep}} = \sigma_a \oplus \sigma_b + Y$ , where  $\sigma_{a,b}$  are bonafide (physically compatible with uncertainty relations [130, Eq. (S5)]) CMs and  $Y$  is any positive semidefinite (PSD) matrix [127, 136, 137]. This decomposition leads naturally to the necessary and sufficient condition for Gaussian state separability [127],

$$\sigma_{\text{sep}} \geq \sigma_a \oplus \sigma_b. \quad (2)$$

Physically,  $Y$  indicates the presence of classically correlated Gaussian noise, and may be considered to be the CM governing a classical mixture of CV first moment displacements within an ensemble.

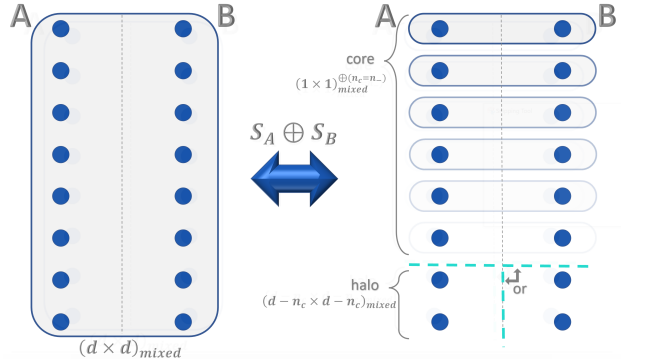


FIG. 1. Diagrammatic representation of consolidating two regions of the vacuum into a distillable negativity core and halo with separability-obscured entanglement. Prior to consolidation (left), the two regions are entangled with multi-mode  $(d \times d)_{\text{mixed}}$  entanglement. After consolidation through local unitary transformation, the negativity is captured in a core of  $(1 \times 1)_{\text{mixed}}$  pairs that manifest the exponential hierarchy in entanglement contributions [130, §S2A]. The dashed (teal) lines indicate two partitions that are individually, but not simultaneously, separable.

As discussed in Ref. [130, §S4], it is possible for the separability designation to obscure the presence of entanglement, i.e., separable states may contain underlying entanglement visible only through additional classical communication or restriction/modification of the noise <sup>2</sup>. The ability of classical noise to obscure entanglement has been observed frequently [138–143], raising cautious concerns for quantum devices required to maintain quantum coherence in its presence.

Due to the lack of uniqueness in convex decompositions of mixed states, inseparable states may be identified as separable upon the addition of noise contributions. Such SOE states have separable density matrices however, their particular convex decompositions require entanglement. This entanglement is invisible to observers within the system, and may only be accessed with the addition of classical communication from the source, e.g., for the post-selection of entangled ensemble samples. However, a restriction of classical correlations upon embedding into a larger QMB system may render this entanglement visible in the density matrix of the whole. In the following, we illustrate a mechanism capable of causing such a restriction, non-simultaneous separability, that leads disjoint regions of the scalar field vacuum to contain this type of SOE.

**Non-Simultaneous Separability** After applying the local, negativity consolidating transformation, disjoint regions of the scalar vacuum are numerically identified to be separable along the core-halo bipartition, and thus expressible as a tensor-product state immersed in Gaussian classical

<sup>1</sup> Numerical values for these quantities are presented in lattice units.

<sup>2</sup> As an interesting example, this mixed decomposition shows that the presence of Gaussian correlations characterized by a tensor product of pure CMs will always result in a separable state, regardless of the entanglement present in the underlying pure state.

correlations,  $Y$ , as

$$\sigma' = \sigma_c \oplus \sigma_h + Y \quad , \quad Y = \begin{pmatrix} \alpha & \beta \\ \beta^T & \delta \end{pmatrix} \quad , \quad (3)$$

with  $Y \geq 0$ . With all the negativity accounted for in the core, the halo degrees of freedom are found to be separable along the A,B region divide,

$$\text{Tr}_c(\sigma') = \sigma_h + \delta = \sigma_{h,A} \oplus \sigma_{h,B} + Y_h \quad . \quad (4)$$

While for pure states, these two observations of sequential separability could be combined to conclude the separability of, for example,  $\sigma_{h,A}$  from the rest of the system, incompatible noise characterizations of  $Y$  and  $Y_h$  limit the viability of such deductions for mixed states. In particular, the negativity between the single-region halo and the rest of the system is found to be non-zero, a sufficient observation for the conclusion of entanglement.

More explicitly, the separability observations of Eqns. (3) and (4) lead to

$$\begin{aligned} \sigma' &= \sigma_c \oplus \sigma_{h,A} \oplus \sigma_{h,B} + Y' \quad , \quad (5) \\ Y' &\equiv \mathbf{0}_c \oplus Y_h - \mathbf{0}_c \oplus \delta + Y \quad , \end{aligned}$$

and three-part simultaneous separability exists for  $Y' \geq 0$ . In contrast, if  $Y' < 0$ , as is observed in the transformed scalar field vacuum, the partitions are not simultaneously separable. This can be physically interpreted as the identification and preservation of core-halo separability (as opposed to tracing of the core) limiting the structure that can be identified as Gaussian noise in the internal halo-halo system. If the individual separability calculations of Eqns. (3) and (4) are satisfied,  $Y$ ,  $Y_h$ , and  $\delta$  are PSD matrices. Upon simplification, a necessary and sufficient condition for simultaneous separability is the identification of Gaussian noise such that,

$$Y' = \begin{pmatrix} \alpha & \beta \\ \beta^T & Y_h \end{pmatrix} \geq 0 \quad , \quad (6)$$

i.e., replacing halo contributions,  $\delta$ , of the Gaussian noise identified in the core-halo partition,  $Y$ , with that compatible with halo<sub>A</sub>-halo<sub>B</sub> separability,  $Y_h$ , must be a valid description of classical Gaussian noise. With this inequality, it is clear how constraints associated with separability observations propagate to subsequent subsystem evaluations of separability. Simultaneous separability may also be addressed through analysis of  $\sigma_h$  alone, as its noise contributions will always be a PSD addition to  $Y$ .

Focusing next on the structure of the core, the additivity of the negativity among the  $(1 \times 1)_{\text{mixed}}$  mode pairs [130, Eq. (S18)] suggests that these core pairs are fully separable from each other. Furthermore, upon tracing, all bipartitions of  $k$ -pairs by  $\ell$ -pairs for  $k + \ell \leq n_c$  are identified to be separable. The remaining question is whether these core pair separability observations are simultaneously compatible with the core-halo separability, i.e., whether the transformed CM can be decomposed as

$$\sigma' = \sigma_{c,1} \oplus \sigma_{c,2} \oplus \cdots \oplus \sigma_{c,n_c} \oplus \sigma_h + Y \quad , \quad (7)$$

where  $\sigma_{c,i}$  is a  $(1_A \times 1_B)_{\text{mixed}}$  CM with non-zero negativity. This question addresses multipartite simultaneous separability of the core pairs. While progress has been made in extending CV separability criteria to tripartite systems [144, 145], the  $(n_c + 1)$ -partite nature of this question is beyond current direct techniques. However, sequential applications of the bipartite procedure of Ref. [146] to  $\sigma_c$  yields a robust approach for numerically identifying viable decompositions in the form of Eq. (7). While not all bipartition sequences yield fully separable decompositions, successful sequences are reliably found for modest sized systems [130, §S3]. Thus, Eq. (7) likely represents the final transformed separability structure after local symplectic negativity consolidation.

**Bound Entanglement in the Field** Through the above exploration, a clear distinction has been made between distillable entanglement localized to the core and BE in the halo. For the latticized field, the latter indicates the presence of BE embedded in an NPT state, though the state is not fully bound as more commonly considered [147–151]. Prior to the development of the transformation presented here, the presence of distillable entanglement in all NPT Gaussian states had been established [122], though the further presence of BE within the NPT scalar field vacuum was unknown.

The non-simultaneous separability within the core-halo system provides one physical picture for understanding the generation of BE [123, 127, 152] as a form of SOE. Defined as the discrepancy between the entanglement required to prepare a quantum state and the entanglement that may be subsequently extracted through distillation, the existence of BE introduces an irreversibility for quantum resources. Separable states that also permit entangled convex decompositions, though quantified to exhibit zero BE by the current definition, provide a clear mechanism for hiding entanglement distributed between two classically-connected parties, uncovered only with additional classical information from the source. When incorporated into many-body quantum states, consistent identification of classical noise contributions may rule out tensor-product convex decompositions that would be viable in isolation, thus demanding the use of an entangled convex decomposition to create an otherwise separable portion of the state.

Shown in Fig. 2, quantification of the SOE in the lattice scalar field vacuum may be achieved through calculation of the  $\sigma_h$  negativity, after identification of classical noise compatible with core-halo separability in Eq. (3). For the purpose of demonstration, we have chosen a mass function,  $m = 3 \times 10^{-3}/d$ , such that the correlation length across the regions is held fixed as  $d$  increases and removes the pixelation. While many solutions in the form of Eq. (3) exist, the decompositions generated by the techniques of Ref. [146] appear to produce a lowest upper bound for the inaccessible region-wise entanglement in the halo. Naturally, the family of decompositions purifying  $\sigma_h$  result in greater values of the halo negativity and further, random perturbations of  $\sigma_h$  satisfying necessary constraints appear also to produce only increases. Thus, this quantity should be interpreted as an estimate of the BE distributed between regions in the halo Hilbert space, with a value of zero incompatible with

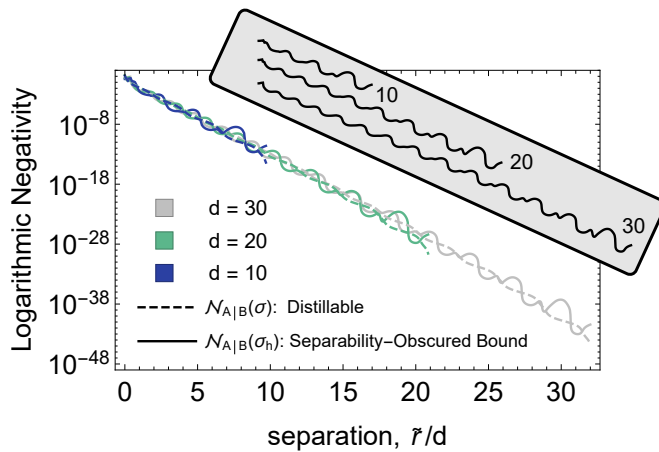


FIG. 2. Logarithmic negativity quantifying distillable and (separability-obscured) bound entanglement between two disjoint regions of the latticized one-dimensional massive ( $m = 0.003/d$ ) scalar field vacuum as a function of dimensionless separation  $\tilde{r}/d$ , where  $\tilde{r}$  is the integer separation in lattice units and  $d$  is the pixelated size of each region. The inset diagrammatically reproduces the SOE (solid lines), vertically displaced to enhance visibility of emergent structure.

non-simultaneous separability.

Figure 2 illustrates that, at fixed region pixelation  $d$  and with the CM techniques developed here, the vanishing of SOE at large separations coincides with the boundary of the corresponding entanglement sphere, i.e., the radii at which the regions become separable [53]. Both the magnitude and exponential decay are consistent with that calculated for the full region negativity [39]. The distillable entanglement and BE fluctuate with amplitudes that diminish toward the continuum limit. The inset of Fig. 2 shows that the regime from which the continuum limit emerges passes through a phase where the SOE exhibits a clear step-wise structure, a feature more commonly found in systems with topological behavior.

**Discussion** By isolating the BE from a collection of  $(1 \times 1)_{\text{mixed}}$  modes carrying the distillable entanglement, the local transformation developed in this work provides an approach for exploring the entanglement structure of mixed QMB systems representing regions of a field. In particular, it illuminates a physical interpretation of BE as SOE within classically-connected subsystems. With relevance beyond the scalar field [130, §S4B], we conjecture that this physical interpretation is encompassing, i.e.,  $\text{BE} \subset \text{SOE}$ , where SOE more broadly incorporates the phenomena of separable states generated with entanglement.

Because explicit convex decompositions necessary to initialize a quantum state directly inform experimental protocols, the entanglement consolidating transformation also allows insight into viable procedures for preparing scalar field vacuum regions in the laboratory. In particular, initializing a pair of latticized scalar vacuum regions can be achieved through distribution of a collection of  $(1 \times 1)_{\text{mixed}}$  entangled modes and a multi-mode separable state that must be generated with a convex decomposition including entanglement. It is of value to note that analogous local unitary

transformations may be applied to  $\sigma_h$  for further consolidation of the BE that must be distributed between the two regions.

Though much progress has been made in simulating the distribution of entanglement utilizing vacuum fields as a medium for (quasi-)particle propagation (e.g., Refs. [153–157]) or in boosted reference frames (e.g., Refs. [29, 30, 158, 159]), techniques capable of reliably extracting spacelike entanglement from the field in the laboratory remain elusive. However, by consolidating the negativity into a core, extraction of the distillable entanglement can be achieved by simply coupling to a reduced number of  $(1 \times 1)$  mode pairs. As such, these methods are expected to elucidate the relevant degrees of freedom, and thus the design of future quantum sensors, capable of recovering spacelike entanglement from continuum quantum fields.

While aspects of these entanglement reorganizations and subsequent conclusions apply more broadly [130, §S2B], it should be stressed that the results do not apply to generic mixed quantum states. However, similar entanglement structures amenable to adapted transformation are expected to exist in regimes of the Standard Model where Gaussian fields provide effective degrees of freedom. The asymptotic freedom of quantum chromodynamics (QCD) in the UV, which provides a perturbative vacuum of quarks and gluons, and chiral symmetry breaking in the IR, which provides a perturbative vacuum of pions, suggests the possibility of non-trivial evolution in the analogous QCD negativity core and halo through the confinement and chiral symmetry breaking scale(s). Hints of interesting behaviors in such symmetry transition regimes, where low-energy effective interactions become increasingly non-local, may be found in the connection between emergent global symmetries and suppressed fluctuations of entanglement, e.g., as displayed in nuclear forces in low-energy scattering [7, 11, 12, 15, 160].

## ACKNOWLEDGMENTS

We would like to thank Silas Beane, Roland Farrell, Neda Hosseiniéhaj, Aidan Murran, and John Preskill for valuable discussions. We would also like to thank the Center for Experimental Nuclear Physics and Astrophysics (CENPA) for providing a creative environment for developmental periods of this work. We have made extensive use of Wolfram Mathematica [161]. DB is supported in part by NSF Nuclear Physics grant PHY-2111046. NK is supported in part by the Walter Burke Institute for Theoretical Physics, and by the U.S. Department of Energy Office of Science, Office of Advanced Scientific Computing Research, (DE-SC0020290), and Office of High Energy Physics DE-AC02-07CH11359. MJS is supported in part by the U.S. Department of Energy, Office of Science, Office of Nuclear Physics, InQuBator for Quantum Simulation (IQuS) under Award Number DOE (NP) Award DE-SC0020970, and was supported in part by the Institute for Nuclear Theory with DOE grant No. DE-FG02-00ER41132. References [162–168] have been cited in the Supplemental Material [130].

---

[1] R. P. Feynman, Simulating physics with computers, *International Journal of Theoretical Physics* **21**, 467 (1982).

[2] C. M. Ho and S. D. H. Hsu, Entanglement and Fast Quantum Thermalization in Heavy Ion Collisions, *Mod. Phys. Lett. A* **31**, 1650110 (2016), arXiv:1506.03696 [hep-th].

[3] D. E. Kharzeev and E. M. Levin, Deep inelastic scattering as a probe of entanglement, *Phys. Rev. D* **95**, 114008 (2017), arXiv:1702.03489 [hep-ph].

[4] O. K. Baker and D. E. Kharzeev, Thermal radiation and entanglement in proton-proton collisions at energies available at the CERN Large Hadron Collider, *Phys. Rev. D* **98**, 054007 (2018), arXiv:1712.04558 [hep-ph].

[5] A. Cervera-Lierta, J. I. Latorre, J. Rojo, and L. Rottoli, Maximal Entanglement in High Energy Physics, *SciPost Phys.* **3**, 036 (2017), arXiv:1703.02989 [hep-th].

[6] J. Berges, S. Floerchinger, and R. Venugopalan, Entanglement and thermalization, *Nucl. Phys. A* **982**, 819 (2019), arXiv:1812.08120 [hep-th].

[7] S. R. Beane, D. B. Kaplan, N. Klco, and M. J. Savage, Entanglement Suppression and Emergent Symmetries of Strong Interactions, *Phys. Rev. Lett.* **122**, 102001 (2019), arXiv:1812.03138 [nucl-th].

[8] O. Gorton and C. W. Johnson, Entanglement entropy and proton-neutron interactions (2019), ESNT workshop on proton-neutron pairing, <http://esnt.cea.fr/Phocea/Page/index.php?id=84>.

[9] S. R. Beane and P. Ehlers, Chiral symmetry breaking, entanglement, and the nucleon spin decomposition, *Mod. Phys. Lett. A* **35**, 2050048 (2019), arXiv:1905.03295 [hep-ph].

[10] Z. Tu, D. E. Kharzeev, and T. Ullrich, Einstein-Podolsky-Rosen Paradox and Quantum Entanglement at Subnucleonic Scales, *Phys. Rev. Lett.* **124**, 062001 (2020), arXiv:1904.11974 [hep-ph].

[11] S. R. Beane and R. C. Farrell, Geometry and entanglement in the scattering matrix, *Annals Phys.* **433**, 168581 (2021), arXiv:2011.01278 [hep-th].

[12] S. R. Beane, R. C. Farrell, and M. Varma, Entanglement minimization in hadronic scattering with pions, *Int. J. Mod. Phys. A* **36**, 2150205 (2021), arXiv:2108.00646 [hep-ph].

[13] D. E. Kharzeev and E. Levin, Deep inelastic scattering as a probe of entanglement: Confronting experimental data, *Phys. Rev. D* **104**, L031503 (2021), arXiv:2102.09773 [hep-ph].

[14] C. Robin, M. J. Savage, and N. Pillet, Entanglement Rearrangement in Self-Consistent Nuclear Structure Calculations, *Phys. Rev. C* **103**, 034325 (2021), arXiv:2007.09157 [nucl-th].

[15] I. Low and T. Mehen, Symmetry from entanglement suppression, (2021), arXiv:2104.10835 [hep-th].

[16] W. Gong, G. Parida, Z. Tu, and R. Venugopalan, Bell-type inequality tests and quantum entanglement from  $\Lambda$ -hyperon spin correlations at high energy colliders, (2021), arXiv:2107.13007 [hep-ph].

[17] A. Roggero, Entanglement and many-body effects in collective neutrino oscillations, *Phys. Rev. D* **104**, 103016 (2021), arXiv:2102.10188 [hep-ph].

[18] N. Mueller, T. V. Zache, and R. Ott, Thermalization of Gauge Theories from their Entanglement Spectrum, (2021), arXiv:2107.11416 [quant-ph].

[19] M. C. Bañuls *et al.*, Simulating Lattice Gauge Theories within Quantum Technologies, *Eur. Phys. J. D* **74**, 165 (2020), arXiv:1911.00003 [quant-ph].

[20] Y. Alexeev *et al.*, Quantum Computer Systems for Scientific Discovery, *P. R. X. Quantum.* **2**, 017001 (2021), arXiv:1912.07577 [quant-ph].

[21] N. Klco, A. Roggero, and M. J. Savage, Standard Model Physics and the Digital Quantum Revolution: Thoughts about the Interface, (2021), arXiv:2107.04769 [quant-ph].

[22] E. Zohar, Quantum simulation of lattice gauge theories in more than one space dimension—requirements, challenges and methods, *Phil. Trans. A. Math. Phys. Eng. Sci.* **380**, 20210069 (2021), arXiv:2106.04609 [quant-ph].

[23] H. Halvorson and R. Clifton, Generic Bell correlation between arbitrary local algebras in quantum field theory, *J. Math. Phys.* **41**, 1711 (2000), arXiv:math-ph/9909013.

[24] H. Reeh and S. Schlieder, Bemerkungen zur unitäräquivalenz von lorentzinvarianten feldern, *Il Nuovo Cimento* (1955-1965) **22**, 1051 (1961).

[25] S. J. Summers and R. Werner, The vacuum violates bell's inequalities, *Physics Letters A* **110**, 257 (1985).

[26] S. J. Summers and R. Werner, Bell's inequalities and quantum field theory. i. general setting, *Journal of Mathematical Physics* **28**, 2440 (1987), <https://doi.org/10.1063/1.527733>.

[27] S. J. Summers and R. Werner, Bell's inequalities and quantum field theory. ii. bell's inequalities are maximally violated in the vacuum, *Journal of Mathematical Physics* **28**, 2448 (1987), <https://doi.org/10.1063/1.527734>.

[28] A. Valentini, Non-local correlations in quantum electrodynamics, *Physics Letters A* **153**, 321 (1991).

[29] B. Reznik, Entanglement from the vacuum, *Found. Phys.* **33**, 167 (2003), arXiv:quant-ph/0212044.

[30] B. Reznik, A. Retzker, and J. Silman, Violating Bell's inequalities in the vacuum, *Phys. Rev. A* **71**, 042104 (2005), arXiv:quant-ph/0310058.

[31] M. Srednicki, Entropy and area, *Phys. Rev. Lett.* **71**, 666 (1993), arXiv:hep-th/9303048 [hep-th].

[32] C. Holzhey, F. Larsen, and F. Wilczek, Geometric and renormalized entropy in conformal field theory, *Nucl. Phys. B* **424**, 443 (1994), arXiv:hep-th/9403108.

[33] C. G. Callan, Jr. and F. Wilczek, On geometric entropy, *Phys. Lett. B* **333**, 55 (1994), arXiv:hep-th/9401072.

[34] K. Audenaert, J. Eisert, M. Plenio, and R. Werner, Entanglement Properties of the Harmonic Chain, *Phys. Rev. A* **66**, 042327 (2002), arXiv:quant-ph/0205025.

[35] A. Botero and B. Reznik, Spatial structures and localization of vacuum entanglement in the linear harmonic chain, *Phys. Rev. A* **70**, 052329 (2004), arXiv:quant-ph/0403233 [quant-ph].

[36] P. Calabrese and J. L. Cardy, Entanglement entropy and quantum field theory, *J. Stat. Mech.* **0406**, P06002 (2004), arXiv:hep-th/0405152.

[37] S. Ryu and T. Takayanagi, Holographic derivation of entanglement entropy from AdS/CFT, *Phys. Rev. Lett.* **96**, 181602 (2006), arXiv:hep-th/0603001.

[38] J. Kofler, V. Vedral, M. S. Kim, and Č. Brukner, Entanglement between collective operators in a linear harmonic chain, *Physical Review A* **73**, 052107 (2006).

[39] S. Marcovitch, A. Retzker, M. Plenio, and B. Reznik, Critical and noncritical long-range entanglement in Klein-Gordon fields, *Phys. Rev. A* **80**, 012325 (2009), arXiv:0811.1288 [quant-ph].

[40] H. Casini and M. Huerta, Entanglement entropy in free quantum field theory, *J. Phys. A* **42**, 504007 (2009),

arXiv:0905.2562 [hep-th].

[41] T. Nishioka, S. Ryu, and T. Takayanagi, Holographic Entanglement Entropy: An Overview, *J. Phys. A* **42**, 504008 (2009), arXiv:0905.0932 [hep-th].

[42] P. Calabrese, J. Cardy, and E. Tonni, Entanglement entropy of two disjoint intervals in conformal field theory, *J. Stat. Mech.* **0911**, P11001 (2009), arXiv:0905.2069 [hep-th].

[43] P. Calabrese and J. Cardy, Entanglement entropy and conformal field theory, *J. Phys. A* **42**, 504005 (2009), arXiv:0905.4013 [cond-mat.stat-mech].

[44] H. Casini, M. Huerta, and R. C. Myers, Towards a derivation of holographic entanglement entropy, *JHEP* **05**, 036, arXiv:1102.0440 [hep-th].

[45] P. Calabrese, J. Cardy, and E. Tonni, Entanglement negativity in quantum field theory, *Phys. Rev. Lett.* **109**, 130502 (2012), arXiv:1206.3092 [cond-mat.stat-mech].

[46] P. Calabrese, J. Cardy, and E. Tonni, Entanglement negativity in extended systems: A field theoretical approach, *J. Stat. Mech.* **1302**, P02008 (2013), arXiv:1210.5359 [cond-mat.stat-mech].

[47] M. R. Mohammadi Mozaffar and A. Mollabashi, Entanglement in Lifshitz-type Quantum Field Theories, *JHEP* **07**, 120, arXiv:1705.00483 [hep-th].

[48] A. Coser, C. De Nobili, and E. Tonni, A contour for the entanglement entropies in harmonic lattices, *Journal of Physics A: Mathematical and Theoretical* **50**, 314001 (2017).

[49] P. Ruggiero, E. Tonni, and P. Calabrese, Entanglement entropy of two disjoint intervals and the recursion formula for conformal blocks, *J. Stat. Mech.* **1811**, 113101 (2018), arXiv:1805.05975 [cond-mat.stat-mech].

[50] G. Di Giulio and E. Tonni, On entanglement hamiltonians of an interval in massless harmonic chains, *J. Stat. Mech.* **2003**, 033102 (2020), arXiv:1911.07188 [cond-mat.stat-mech].

[51] N. Klco and M. J. Savage, Geometric quantum information structure in quantum fields and their lattice simulation, *Phys. Rev. D* **103**, 065007 (2021), arXiv:2008.03647 [quant-ph].

[52] A. Roy, F. Pollmann, and H. Saleur, Entanglement Hamiltonian of the 1+1-dimensional free, compactified boson conformal field theory, *J. Stat. Mech.* **2008**, 083104 (2020), arXiv:2004.14370 [cond-mat.stat-mech].

[53] N. Klco and M. J. Savage, Entanglement Spheres and a UV-IR Connection in Effective Field Theories, *Phys. Rev. Lett.* **127**, 211602 (2021), arXiv:2103.14999 [hep-th].

[54] H. Wang, M. P. Blencowe, C. M. Wilson, and A. J. Rimberg, Mechanically generating entangled photons from the vacuum: A microwave circuit-acoustic resonator analog of the oscillatory Unruh effect, *Phys. Rev. A* **99**, 053833 (2019), arXiv:1811.10065 [quant-ph].

[55] A. Roy, D. Schuricht, J. Hauschild, F. Pollmann, and H. Saleur, The quantum sine-Gordon model with quantum circuits, *Nucl. Phys. B* **968**, 115445 (2021), arXiv:2007.06874 [quant-ph].

[56] J. S. C. Hung, J. H. Busnaina, C. W. S. Chang, A. M. Vadiraj, I. Nsanzineza, E. Solano, H. Alaeian, E. Rico, and C. M. Wilson, Quantum simulation of the bosonic creutz ladder with a parametric cavity, *Physical Review Letters* **127**, 10.1103/physrevlett.127.100503 (2021).

[57] A. Kitaev and W. A. Webb, Wavefunction preparation and resampling using a quantum computer, (2009), arXiv:0801.0342 [quant-ph].

[58] S. P. Jordan, K. S. M. Lee, and J. Preskill, Quantum Computation of Scattering in Scalar Quantum Field Theories, *Quant. Inf. Comput.* **14**, 1014 (2014), arXiv:1112.4833 [hep-th].

[59] S. P. Jordan, K. S. M. Lee, and J. Preskill, Quantum Algorithms for Quantum Field Theories, *Science* **336**, 1130 (2012), arXiv:1111.3633 [quant-ph].

[60] K. Marshall, R. Pooser, G. Siopsis, and C. Weedbrook, Quantum simulation of quantum field theory using continuous variables, *Phys. Rev. A* **92**, 063825 (2015), arXiv:1503.08121 [quant-ph].

[61] A. Bermudez, G. Aarts, and M. Müller, Quantum sensors for the generating functional of interacting quantum field theories, *Phys. Rev. X* **7**, 041012 (2017), arXiv:1704.02877 [quant-ph].

[62] K. Yeter-Aydeniz and G. Siopsis, Quantum Computation of Scattering Amplitudes in Scalar Quantum Electrodynamics, *Phys. Rev. D* **97**, 036004 (2018), arXiv:1709.02355 [quant-ph].

[63] N. Klco and M. J. Savage, Digitization of scalar fields for quantum computing, *Phys. Rev. A* **99**, 052335 (2019), arXiv:1808.10378 [quant-ph].

[64] A. Macridin, P. Spentzouris, J. Amundson, and R. Harnik, Digital quantum computation of fermion-boson interacting systems, *Phys. Rev. A* **98**, 042312 (2018), arXiv:1805.09928 [quant-ph].

[65] K. Yeter-Aydeniz, E. F. Dumitrescu, A. J. McCaskey, R. S. Bennink, R. C. Pooser, and G. Siopsis, Scalar quantum field theories as a benchmark for near-term quantum computers, *Phys. Rev. A* **99**, 032306 (2019).

[66] N. Klco and M. J. Savage, Systematically Localizable Operators for Quantum Simulations of Quantum Field Theories, *Phys. Rev. A* **102**, 012619 (2020), arXiv:1912.03577 [quant-ph].

[67] N. Klco and M. J. Savage, Fixed-point quantum circuits for quantum field theories, *Phys. Rev. A* **102**, 052422 (2020), arXiv:2002.02018 [quant-ph].

[68] J. a. Barata, N. Mueller, A. Tarasov, and R. Venugopalan, Single-particle digitization strategy for quantum computation of a  $\phi^4$  scalar field theory, *Phys. Rev. A* **103**, 042410 (2021), arXiv:2012.00020 [hep-th].

[69] A. Macridin, A. C. Y. Li, S. Mrenna, and P. Spentzouris, Bosonic field digitization for quantum computers, (2021), arXiv:2108.10793 [quant-ph].

[70] D. M. Kurkcuoglu, M. S. Alam, A. C. Y. Li, A. Macridin, and G. N. Perdue, Quantum simulation of  $\phi^4$  theories in qudit systems, (2021), arXiv:2108.13357 [quant-ph].

[71] P. Deliyannis, M. Freytsis, B. Nachman, and C. W. Bauer, Practical considerations for the preparation of multivariate Gaussian states on quantum computers, (2021), arXiv:2109.10918 [quant-ph].

[72] T. Byrnes and Y. Yamamoto, Simulating lattice gauge theories on a quantum computer, *Phys. Rev. A* **73**, 022328 (2006).

[73] E. Zohar, J. I. Cirac, and B. Reznik, Cold-Atom Quantum Simulator for SU(2) Yang-Mills Lattice Gauge Theory, *Phys. Rev. Lett.* **110**, 125304 (2013), arXiv:1211.2241 [quant-ph].

[74] D. Banerjee, M. Bögli, M. Dalmonte, E. Rico, P. Strelber, U. J. Wiese, and P. Zoller, Atomic Quantum Simulation of U(N) and SU(N) Non-Abelian Lattice Gauge Theories, *Phys. Rev. Lett.* **110**, 125303 (2013), arXiv:1211.2242 [cond-mat.quant-gas].

[75] L. Tagliacozzo, A. Celi, P. Orland, and M. Lewenstein, Simulations of non-Abelian gauge theories with optical lattices, *Nature Commun.* **4**, 2615 (2013), arXiv:1211.2704 [cond-mat.quant-gas].

[76] K. Stannigel, P. Hauke, D. Marcos, M. Hafezi, S. Diehl,

M. Dalmonte, and P. Zoller, Constrained dynamics via the Zeno effect in quantum simulation: Implementing non-Abelian lattice gauge theories with cold atoms, *Phys. Rev. Lett.* **112**, 120406 (2014), arXiv:1308.0528 [quant-ph].

[77] E. Zohar, J. I. Cirac, and B. Reznik, Quantum simulations of gauge theories with ultracold atoms: local gauge invariance from angular momentum conservation, *Phys. Rev. A* **88**, 023617 (2013), arXiv:1303.5040 [quant-ph].

[78] E. Zohar and M. Burrello, Formulation of lattice gauge theories for quantum simulations, *Phys. Rev. D* **91**, 054506 (2015), arXiv:1409.3085 [quant-ph].

[79] V. Kasper, F. Hebenstreit, M. Oberthaler, and J. Berges, Schwinger pair production with ultracold atoms, *Phys. Lett. B* **760**, 742 (2016), arXiv:1506.01238 [cond-mat.quant-gas].

[80] A. Mezzacapo, E. Rico, C. Sabín, I. L. Egusquiza, L. Lamata, and E. Solano, Non-Abelian  $SU(2)$  Lattice Gauge Theories in Superconducting Circuits, *Phys. Rev. Lett.* **115**, 240502 (2015), arXiv:1505.04720 [quant-ph].

[81] A. Bazavov, Y. Meurice, S.-W. Tsai, J. Unmuth-Yockey, and J. Zhang, Gauge-invariant implementation of the Abelian Higgs model on optical lattices, *Phys. Rev. D* **92**, 076003 (2015), arXiv:1503.08354 [hep-lat].

[82] E. A. Martinez *et al.*, Real-time dynamics of lattice gauge theories with a few-qubit quantum computer, *Nature* **534**, 516 (2016), arXiv:1605.04570 [quant-ph].

[83] D. González-Cuadra, E. Zohar, and J. I. Cirac, Quantum Simulation of the Abelian-Higgs Lattice Gauge Theory with Ultracold Atoms, *New J. Phys.* **19**, 063038 (2017), arXiv:1702.05492 [quant-ph].

[84] E. Zohar and J. I. Cirac, Eliminating fermionic matter fields in lattice gauge theories, *Phys. Rev. B* **98**, 075119 (2018), arXiv:1805.05347 [quant-ph].

[85] I. Raychowdhury and J. R. Stryker, Solving Gauss's Law on Digital Quantum Computers with Loop-String-Hadron Digitization, *Phys. Rev. Res.* **2**, 033039 (2020), arXiv:1812.07554 [hep-lat].

[86] J. R. Stryker, Oracles for Gauss's law on digital quantum computers, *Phys. Rev. A* **99**, 042301 (2019), arXiv:1812.01617 [quant-ph].

[87] E. Zohar and J. I. Cirac, Removing Staggered Fermionic Matter in  $U(N)$  and  $SU(N)$  Lattice Gauge Theories, *Phys. Rev. D* **99**, 114511 (2019), arXiv:1905.00652 [quant-ph].

[88] T. V. Zache, T. Schweigler, S. Erne, J. Schmiedmayer, and J. Berges, Extracting the field theory description of a quantum many-body system from experimental data, *Phys. Rev. X* **10**, 011020 (2020), arXiv:1909.12815 [cond-mat.quant-gas].

[89] A. Alexandru, P. F. Bedaque, S. Harmalkar, H. Lamm, S. Lawrence, and N. C. Warrington (NuQS), Gluon Field Digitization for Quantum Computers, *Phys. Rev. D* **100**, 114501 (2019), arXiv:1906.11213 [hep-lat].

[90] H. Singh and S. Chandrasekharan, Qubit regularization of the  $O(3)$  sigma model, *Phys. Rev. D* **100**, 054505 (2019), arXiv:1905.13204 [hep-lat].

[91] D. Luo, J. Shen, M. Highman, B. K. Clark, B. DeMarco, A. X. El-Khadra, and B. Gadway, Framework for simulating gauge theories with dipolar spin systems, *Phys. Rev. A* **102**, 032617 (2020), arXiv:1912.11488 [quant-ph].

[92] F. M. Surace, P. P. Mazza, G. Giudici, A. Lerose, A. Gambassi, and M. Dalmonte, Lattice gauge theories and string dynamics in Rydberg atom quantum simulators, *Phys. Rev. X* **10**, 021041 (2020), arXiv:1902.09551 [cond-mat.quant-gas].

[93] N. Klco, J. R. Stryker, and M. J. Savage,  $SU(2)$  non-Abelian gauge field theory in one dimension on digital quantum computers, *Phys. Rev. D* **101**, 074512 (2020), arXiv:1908.06935 [quant-ph].

[94] A. Mil, T. V. Zache, A. Hegde, A. Xia, R. P. Bhatt, M. K. Oberthaler, P. Hauke, J. Berges, and F. Jendrzejewski, A scalable realization of local  $U(1)$  gauge invariance in cold atomic mixtures, *Science* **367**, 1128 (2020), arXiv:1909.07641 [cond-mat.quant-gas].

[95] R. Ott, T. V. Zache, F. Jendrzejewski, and J. Berges, Scalable Cold-Atom Quantum Simulator for Two-Dimensional QED, *Phys. Rev. Lett.* **127**, 130504 (2021), arXiv:2012.10432 [cond-mat.quant-gas].

[96] J. F. Haase, L. Dellantonio, A. Celi, D. Paulson, A. Kan, K. Jansen, and C. A. Muschik, A resource efficient approach for quantum and classical simulations of gauge theories in particle physics, *Quantum* **5**, 393 (2021), arXiv:2006.14160 [quant-ph].

[97] R. Dasgupta and I. Raychowdhury, Cold Atom Quantum Simulator for String and Hadron Dynamics in Non-Abelian Lattice Gauge Theory, (2020), arXiv:2009.13969 [hep-lat].

[98] A. F. Shaw, P. Lougovski, J. R. Stryker, and N. Wiebe, Quantum Algorithms for Simulating the Lattice Schwinger Model, *Quantum* **4**, 306 (2020).

[99] A. J. Buser, H. Gharibyan, M. Hanada, M. Honda, and J. Liu, Quantum simulation of gauge theory via orbifold lattice, *JHEP* **09**, 034, arXiv:2011.06576 [hep-th].

[100] J. Shen, D. Luo, M. Highman, B. K. Clark, B. DeMarco, A. X. El-Khadra, and B. Gadway, (1+1)-d  $U(1)$  Quantum link models from effective Hamiltonians of dipolar molecules, *PoS LATTICE2019*, 125 (2020), arXiv:2001.10002 [hep-lat].

[101] F. M. Surace, P. P. Mazza, G. Giudici, A. Lerose, A. Gambassi, and M. Dalmonte, Lattice gauge theories and string dynamics in rydberg atom quantum simulators, *Physical Review X* **10**, 10.1103/physrevx.10.021041 (2020).

[102] M. Van Damme, J. C. Halimeh, and P. Hauke, Gauge-Symmetry Violation Quantum Phase Transition in Lattice Gauge Theories, (2020), arXiv:2010.07338 [cond-mat.quant-gas].

[103] B. Yang, H. Sun, R. Ott, H.-Y. Wang, T. V. Zache, J. C. Halimeh, Z.-S. Yuan, P. Hauke, and J.-W. Pan, Observation of gauge invariance in a 71-site bose–hubbard quantum simulator, *Nature* **587**, 392–396 (2020).

[104] M. Kreshchuk, W. M. Kirby, G. Goldstein, H. Beuken, and P. J. Love, Quantum Simulation of Quantum Field Theory in the Light-Front Formulation, (2020), arXiv:2002.04016 [quant-ph].

[105] V. Kasper, G. Juzeliunas, M. Lewenstein, F. Jendrzejewski, and E. Zohar, From the Jaynes–Cummings model to non-abelian gauge theories: a guided tour for the quantum engineer, *New J. Phys.* **22**, 103027 (2020), arXiv:2006.01258 [quant-ph].

[106] M. Kreshchuk, S. Jia, W. M. Kirby, G. Goldstein, J. P. Vary, and P. J. Love, Simulating Hadronic Physics on NISQ devices using Basis Light-Front Quantization, *Phys. Rev. A* **103**, 062601 (2021), arXiv:2011.13443 [quant-ph].

[107] V. Kasper, T. V. Zache, F. Jendrzejewski, M. Lewenstein, and E. Zohar, Non-Abelian gauge invariance from dynamical decoupling, (2020), arXiv:2012.08620 [quant-ph].

[108] U.-J. Wiese, Quantum Link Models for the Quantum Simulation of Gauge Theories, (2020), accessed: 2021-05-31.

[109] Z. Davoudi, I. Raychowdhury, and A. Shaw, Search for efficient formulations for Hamiltonian simulation of non-Abelian lattice gauge theories, *Phys. Rev. D* **104**, 074505 (2021), arXiv:2009.11802 [hep-lat].

[110] A. Ciavarella, N. Klco, and M. J. Savage, Trailhead for quantum simulation of  $SU(3)$  Yang–Mills lattice gauge the-

ory in the local multiplet basis, *Phys. Rev. D* **103**, 094501 (2021), arXiv:2101.10227 [quant-ph].

[111] C. W. Bauer, M. Freytsis, and B. Nachman, Simulating Collider Physics on Quantum Computers Using Effective Field Theories, *Phys. Rev. Lett.* **127**, 212001 (2021), arXiv:2102.05044 [hep-ph].

[112] N. Klco and M. J. Savage, Hierarchical qubit maps and hierarchically implemented quantum error correction, *Phys. Rev. A* **104**, 062425 (2021), arXiv:2109.01953 [quant-ph].

[113] J. R. Stryker, Shearing approach to gauge invariant Trotterization, (2021), arXiv:2105.11548 [hep-lat].

[114] Z. Davoudi, N. M. Linke, and G. Pagano, Toward simulating quantum field theories with controlled phonon-ion dynamics: A hybrid analog-digital approach, *Phys. Rev. Res.* **3**, 043072 (2021), arXiv:2104.09346 [quant-ph].

[115] Y. Atas, J. Zhang, R. Lewis, A. Jahanpour, J. F. Haase, and C. A. Muschik, SU(2) hadrons on a quantum computer, (2021), arXiv:2102.08920 [quant-ph].

[116] S. A. Rahman, R. Lewis, E. Mendicelli, and S. Powell, SU(2) lattice gauge theory on a quantum annealer, *Phys. Rev. D* **104**, 034501 (2021), arXiv:2103.08661 [hep-lat].

[117] M. Aيدلسبرغر, L. Barbiero, A. Bermudez, T. Chanda, A. Dauphin, D. González-Cuadra, P. R. Grzybowski, S. Hands, F. Jendrzejewski, J. Jünemann, G. Juzeliunas, V. Kasper, A. Piga, S.-J. Ran, M. Rizzi, G. Sierra, L. Tagliacozzo, E. Tirrito, T. V. Zache, J. Zakrzewski, E. Zohar, and M. Lewenstein, Cold atoms meet lattice gauge theory, arXiv preprint arXiv:2106.03063 (2021).

[118] M. Horodecki, P. Horodecki, and R. Horodecki, On the necessary and sufficient conditions for separability of mixed quantum states, *Phys. Lett. A* **223**, 1 (1996), arXiv:quant-ph/9605038.

[119] G. Vidal and R. Werner, Computable measure of entanglement, *Phys. Rev. A* **65**, 032314 (2002), arXiv:quant-ph/0102117.

[120] R. Simon, Peres-Horodecki Separability Criterion for Continuous Variable Systems, *Phys. Rev. Lett.* **84**, 2726 (2000), arXiv:quant-ph/9909044.

[121] M. B. Plenio, Logarithmic Negativity: A Full Entanglement Monotone That is not Convex, *Phys. Rev. Lett.* **95**, 090503 (2005), arXiv:quant-ph/0505071.

[122] G. Giedke, L.-M. Duan, J. I. Cirac, and P. Zoller, Distillability criterion for all bipartite gaussian states, *Quantum Information and Computation* **1**, 79 (2001), arXiv:quant-ph/0104072 [quant-ph].

[123] M. Horodecki, P. Horodecki, and R. Horodecki, Mixed-state entanglement and distillation: Is there a “bound” entanglement in nature?, *Phys. Rev. Lett.* **80**, 5239 (1998).

[124] C. H. Bennett, D. P. DiVincenzo, T. Mor, P. W. Shor, J. A. Smolin, and B. M. Terhal, Unextendible Product Bases and Bound Entanglement, *Phys. Rev. Lett.* **82**, 5385 (1999), arXiv:quant-ph/9808030 [quant-ph].

[125] D. Bruß and A. Peres, Construction of quantum states with bound entanglement, *Phys. Rev. A* **61**, 030301 (2000), arXiv:quant-ph/9911056 [quant-ph].

[126] J. A. Smolin, Four-party unlockable bound entangled state, *Phys. Rev. A* **63**, 032306 (2001), arXiv:quant-ph/0001001 [quant-ph].

[127] R. F. Werner and M. M. Wolf, Bound Entangled Gaussian States, *Phys. Rev. Lett.* **86**, 3658 (2001), arXiv:quant-ph/0009118 [quant-ph].

[128] H.-P. Breuer, Optimal Entanglement Criterion for Mixed Quantum States, *Phys. Rev. Lett.* **97**, 080501 (2006), arXiv:quant-ph/0605036 [quant-ph].

[129] M. Piani and C. E. Mora, Class of positive-partial-transpose bound entangled states associated with almost any set of pure entangled states, *Physical Review A* **75**, 10.1103/physreva.75.012305 (2007).

[130] N. Klco, D. H. Beck, and M. J. Savage, Supplementary material: Entanglement structures in quantum field theories: Negativity cores and bound entanglement in the vacuum, (2021).

[131] L.-M. Duan, G. Giedke, J. I. Cirac, and P. Zoller, Inseparability criterion for continuous variable systems, *Physical Review Letters* **84**, 2722–2725 (2000).

[132] G. Giedke, L.-M. Duan, J. I. Cirac, and P. Zoller, All inseparable two-mode Gaussian continuous variable states are distillable, arXiv e-prints , quant-ph/0007061 (2000), arXiv:quant-ph/0007061 [quant-ph].

[133] A. Botero and B. Reznik, Modewise entanglement of Gaussian states, *Phys. Rev. A* **67**, 052311 (2003), arXiv:quant-ph/0209026 [quant-ph].

[134] A. Serafini, G. Adesso, and F. Illuminati, Unitarily localizable entanglement of gaussian states, *Physical Review A* **71**, 10.1103/physreva.71.032349 (2005).

[135] M. M. Wolf, Not-So-Normal Mode Decomposition, *Phys. Rev. Lett.* **100**, 070505 (2008), arXiv:0707.0604 [quant-ph].

[136] L. Lami, A. Serafini, and G. Adesso, Gaussian entanglement revisited, *New Journal of Physics* **20**, arXiv:1612.05215 (2018), arXiv:1612.05215 [quant-ph].

[137] A. Serafini, *Quantum Continuous Variables: A Primer of Theoretical Methods* (CRC Press, 2017).

[138] O. Cohen, Unlocking hidden entanglement with classical information, *Phys. Rev. Lett.* **80**, 2493 (1998).

[139] A. Sanpera, R. Tarrach, and G. Vidal, Local description of quantum inseparability, *Phys. Rev. A* **58**, 826 (1998).

[140] G. Vidal and R. Tarrach, Robustness of entanglement, *Phys. Rev. A* **59**, 141 (1999), arXiv:quant-ph/9806094.

[141] J. A. Smolin, Four-party unlockable bound entangled state, *Phys. Rev. A* **63**, 032306 (2001).

[142] T. Yu and J. Eberly, Sudden death of entanglement: Classical noise effects, *Optics Communications* **264**, 393–397 (2006).

[143] T. Yu and J. H. Eberly, Sudden death of entanglement, *Science* **323**, 598–601 (2009).

[144] G. Giedke, B. Kraus, M. Lewenstein, and J. I. Cirac, Separability properties of three-mode gaussian states, *Physical Review A* **64**, 10.1103/physreva.64.052303 (2001).

[145] G. Adesso, A. Serafini, and F. Illuminati, Multipartite entanglement in three-mode gaussian states of continuous-variable systems: Quantification, sharing structure, and decoherence, *Physical Review A* **73**, 10.1103/physreva.73.032345 (2006).

[146] G. Giedke, B. Kraus, M. Lewenstein, and J. I. Cirac, Entanglement Criteria for All Bipartite Gaussian States, *Phys. Rev. Lett.* **87**, quant-ph/0104050 (2001), arXiv:quant-ph/0104050 [quant-ph].

[147] W. Dür, J. I. Cirac, M. Lewenstein, and D. Bruß, Distillability and partial transposition in bipartite systems, *Phys. Rev. A* **61**, 062313 (2000), arXiv:quant-ph/9910022 [quant-ph].

[148] D. P. DiVincenzo, P. W. Shor, J. A. Smolin, B. M. Terhal, and A. V. Thapliyal, Evidence for bound entangled states with negative partial transpose, *Physical Review A* **61**, 10.1103/physreva.61.062312 (2000).

[149] R. Simon, NPPT Bound Entanglement Exists, arXiv e-prints , quant-ph/0608250 (2006), arXiv:quant-ph/0608250 [quant-ph].

[150] I. Chattopadhyay and D. Sarkar, NPT Bound Entanglement- The Problem Revisited, arXiv e-prints , quant-ph/0609050 (2006), arXiv:quant-ph/0609050 [quant-ph].

[151] L. Pankowski, M. Piani, M. Horodecki, and P. Horodecki, A few steps more towards npt bound entanglement, *IEEE Transactions on Information Theory* **56**, 4085–4100 (2010).

[152] P. Horodecki and M. Lewenstein, Bound entanglement and continuous variables, *Phys. Rev. Lett.* **85**, 2657 (2000).

[153] A. Retzker, J. I. Cirac, and B. Reznik, Detecting vacuum entanglement in a linear ion trap, *Physical Review Letters* **94**, 10.1103/physrevlett.94.050504 (2005).

[154] E. Martin-Martinez, E. G. Brown, W. Donnelly, and A. Kempf, Sustainable entanglement production from a quantum field, *Physical Review A* **88**, 10.1103/physreva.88.052310 (2013).

[155] A. Pozas-Kerstjens and E. Martin-Martinez, Entanglement harvesting from the electromagnetic vacuum with hydrogenlike atoms, *Physical Review D* **94**, 10.1103/physrevd.94.064074 (2016).

[156] A. Pozas-Kerstjens, J. Louko, and E. Martin-Martinez, Degenerate detectors are unable to harvest spacelike entanglement, *Physical Review D* **95**, 10.1103/physrevd.95.105009 (2017).

[157] P. Simidzija, R. H. Jonsson, and E. Martin-Martinez, General no-go theorem for entanglement extraction, *Physical Review D* **97**, 10.1103/physrevd.97.125002 (2018).

[158] W. G. Unruh, Notes on black-hole evaporation, *Phys. Rev. D* **14**, 870 (1976).

[159] G. Salton, R. B. Mann, and N. C. Menicucci, Acceleration-assisted entanglement harvesting and rangefinding, *New Journal of Physics* **17**, 035001 (2015).

[160] M. L. Wagman, F. Winter, E. Chang, Z. Davoudi, W. Detmold, K. Orginos, M. J. Savage, and P. E. Shanahan, Baryon-Baryon Interactions and Spin-Flavor Symmetry from Lattice Quantum Chromodynamics, *Phys. Rev. D* **96**, 114510 (2017), arXiv:1706.06550 [hep-lat].

[161] Wolfram Research, Inc., *Mathematica, Version 11.1*, champaign, IL, 2020.

[162] J. Williamson, On the algebraic problem concerning the normal forms of linear dynamical systems, *American Journal of Mathematics* **58**, 141 (1936), full publication date: Jan., 1936.

[163] F. Pastawski, B. Yoshida, D. Harlow, and J. Preskill, Holographic quantum error-correcting codes: Toy models for the bulk/boundary correspondence, *JHEP* **06**, 149, arXiv:1503.06237 [hep-th].

[164] R. F. Werner, Quantum states with einstein-podolsky-rosen correlations admitting a hidden-variable model, *Phys. Rev. A* **40**, 4277 (1989).

[165] M. Horodecki and P. Horodecki, Reduction criterion of separability and limits for a class of distillation protocols, *Phys. Rev. A* **59**, 4206 (1999), arXiv:quant-ph/9708015.

[166] H. Ollivier and W. H. Zurek, Quantum discord: A measure of the quantumness of correlations, *Phys. Rev. Lett.* **88**, 017901 (2001).

[167] A. Ferraro, L. Aolita, D. Cavalcanti, F. M. Cucchietti, and A. Acín, Almost all quantum states have nonclassical correlations, *Phys. Rev. A* **81**, 052318 (2010).

[168] M. Poxleitner and H. Hinrichsen, Gaussian continuous-variable isotropic state, *Phys. Rev. A* **104**, 032423 (2021), arXiv:2105.03141 [quant-ph].

# Supplemental Material

## Entanglement Structures in Quantum Field Theories: Negativity Cores and Bound Entanglement in the Vacuum

Natalie Klco,<sup>1,\*</sup> D. H. Beck,<sup>2,†</sup> and Martin J. Savage<sup>3,‡</sup><sup>1</sup>*Institute for Quantum Information and Matter and Walter Burke Institute for Theoretical Physics,  
California Institute of Technology, Pasadena CA 91125, USA*<sup>2</sup>*Department of Physics and Illinois Quantum Information Science and Technology (IQUIST) Center,  
University of Illinois at Urbana-Champaign, Urbana, IL 61801, USA*<sup>3</sup>*InQubator for Quantum Simulation (IQuS), Department of Physics,  
University of Washington, Seattle, WA 98195, USA*

(Dated: February 10, 2022 - 2:21)

### CONTENTS

S1. Gaussian Formulation of Lattice Scalar Field Vacuum Regions	10
S2. Manifestation of Negativity Cores through Local Transformation	11
A. Structure of Negativity Core	12
B. Explicit Construction of Local Transformation	13
C. Symplectic Gram Schmidt	14
D. Examples: Entanglement Consolidation in the Vacuum	15
1. $GH^\Gamma$ Eigenvectors	15
2. $i\Omega\sigma^\Gamma$ Eigenvectors	16
S3. The Gaussian Separability Criterion	17
S4. Separability-Obscured Entanglement (SOE)	19
A. Example: SOE in the Lattice Scalar Field Vacuum	19
B. Separability-Obscured Entanglement and Bound Entanglement	21
S5. Numerical Tables	22

### S1. GAUSSIAN FORMULATION OF LATTICE SCALAR FIELD VACUUM REGIONS

The free lattice scalar field defined by a quadratic Hamiltonian can be represented naturally by a family of Gaussian states. In this formalism, CV density matrices are uniquely characterized by  $2n$ -dimensional CMs for a lattice of  $n$  sites. In the basis of field and conjugate momentum operators  $\mathbf{r} = \{\phi_1, \pi_1, \phi_2, \pi_2, \dots, \phi_n, \pi_n\}$ , matrix elements of the ground state CM are defined by the two-point vacuum expectation values,

$$\sigma_{i,j} = 2\langle r_i r_j \rangle \quad . \quad (\text{S1})$$

With vanishing  $\langle \phi_i \pi_j \rangle$  expectation values in the vacuum, the CM is an interleaved version of the following dense matrices of two-point correlation functions,

$$G_{i,j} = \langle \phi_i \phi_j \rangle \quad , \quad H_{i,j} = \langle \pi_i \pi_j \rangle \quad . \quad (\text{S2})$$

Analytic expressions for the two point correlators in one and two spatial dimensions have been provided in Refs. [35, 48, 53]. A symplectic matrix,  $\Omega$ , encodes the commutation relations,

$$[\mathbf{r}, \mathbf{r}^T] = i\Omega_n \quad , \quad \Omega_n = \bigoplus_{j=1}^n i\tau_y \quad , \quad (\text{S3})$$

---

\* [natklco@caltech.edu](mailto:natklco@caltech.edu)

† [dhbeck@illinois.edu](mailto:dhbeck@illinois.edu)

‡ [mjs5@uw.edu](mailto:mjs5@uw.edu); On leave from the Institute for Nuclear Theory.

with  $\tau_y$  the second Pauli matrix. These commutation relations are, by construction, invariant under symplectic transformations,  $S$ ,

$$S\Omega S^T = \Omega \quad , \quad S \in Sp(2n, \mathbb{R}) \quad . \quad (\text{S4})$$

As such, unitary operations on the Hilbert space become symplectic operations on the CM phase space. The positive definiteness of density matrices and adherence to the canonical commutation relations is expressed in phase space as the criterion,

$$\sigma - i\Omega \geq 0 \quad , \quad (\text{S5})$$

a necessary and sufficient condition for a CM to be physical. Through global symplectic operations spanning the space, every CM can be diagonalized to the Williamson normal form [162],

$$\sigma = S \left( \bigoplus_{j=1}^n \nu_j \mathbb{I}_2 \right) S^T \quad , \quad (\text{S6})$$

where the diagonal elements  $\nu_j \geq 1$  are the symplectic eigenvalues, invariants under symplectic transformations characterizing the state. If  $\nu_j = 1 \forall j$ , the state is pure. While a constructive determination of the symplectic transformation to the Williamson normal form is possible, the spectrum of symplectic eigenvalues may be calculated as,

$$\nu = \text{spec}|i\Omega\sigma| = 2 \text{spec}\sqrt{GH} \quad , \quad (\text{S7})$$

where the first spectrum contains a doubling of eigenvalues symmetrically distributed about zero.

The CV partial transposition (PT) operation negates the conjugate momentum operators on one side of the chosen mode bipartition [120]. For  $n_{a,b}$  modes on either side of the bipartition, this may be implemented through the transformation  $\sigma^\Gamma = \Gamma \sigma \Gamma$  with

$$\Gamma = \left( \bigoplus_{j=1}^{n_a} \mathbb{I}_2 \right) \oplus \left( \bigoplus_{j=n_a+1}^{n_a+n_b} \text{diag}(1, -1) \right) \quad . \quad (\text{S8})$$

Note that  $\Gamma$  is not symplectic (and thus not a unitary operation in the Hilbert space) such that the symplectic spectrum is not invariant under this map,

$$\nu^\Gamma = \text{spec}|i\Omega\sigma^\Gamma| = 2\text{spec}\sqrt{GH^\Gamma} \quad , \quad (\text{S9})$$

and symplectic eigenvalues  $\nu_i^\Gamma < 1$  indicate inseparability. As can be seen by the structure of Eq. (S6), the symplectic eigenvalues characterize the system by a set of thermal states functioning as normal modes in phase space. The logarithmic negativity is additive in the basis of PT normal modes, and completely characterized by the PT symplectic eigenvalues

$$\mathcal{N} = - \sum_{j=1}^n \log_2 \min(\nu_i^\Gamma, 1) \equiv \sum_{j=1}^n \mathcal{N}_j \quad , \quad (\text{S10})$$

$$= - \sum_{j=1}^{n_-} \log_2 \nu_i^\Gamma \quad , \quad (\text{S11})$$

where  $n_-$  is the number of symplectic eigenvalues less than 1.

## S2. MANIFESTATION OF NEGATIVITY CORES THROUGH LOCAL TRANSFORMATION

In order to reveal the presence of BE between regions of the vacuum that also exhibit distillable entanglement, we have developed a local reorganization of the quantum information in each region. Broadly, the value of reorganizing entanglement into reduced mode configurations is multifaceted e.g., computationally accessible entanglement measures may become both necessary and sufficient, distillation and extraction protocols may become clear and reliably available, and state preparation procedures may become amenable for implementation in low-connectivity environments.

In the landscape of continuous variable (CV) quantum systems, such as the spatially latticized scalar field, a number of entanglement structure transformations are known. For example, any  $(\ell \times n)_{\text{mixed}}$  state with a permutation symmetry among the modes  $\ell$  (monosymmetric) can be transformed to a  $(1 \times n)_{\text{mixed}}$  state and a set of  $(\ell - 1)$  unentangled single modes [136, 137]. This reorganization associates  $(\ell \times n)_{\text{mixed}}$  monosymmetric Gaussian states with the convenient features of  $(1 \times n)_{\text{mixed}}$

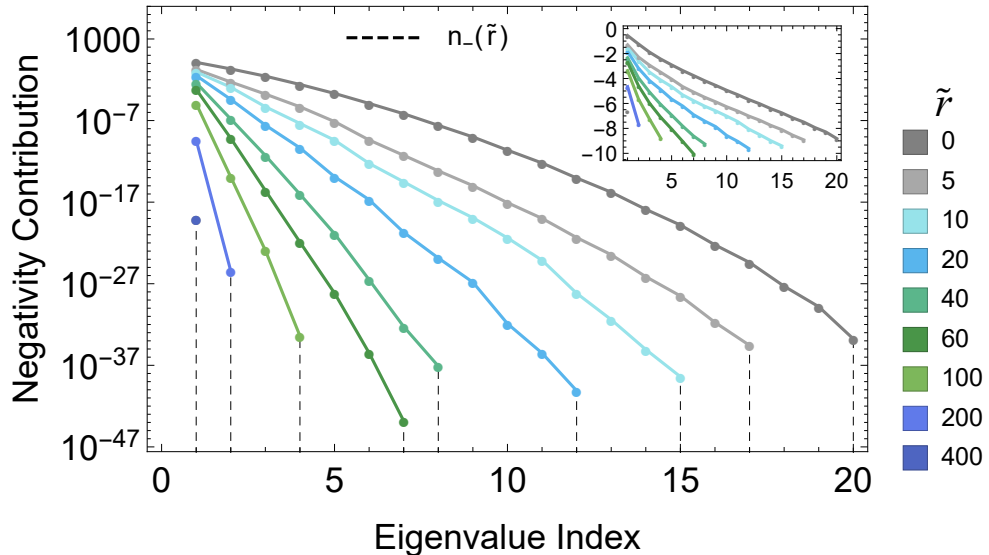


FIG. S1. Logarithmic negativity contributions for distillable entanglement between vacuum regions of the one-dimensional massive scalar field with  $d = 30$  and  $m = 0.003$  as a function of partially transposed symplectic eigenvalue index for a series of separations,  $\tilde{r}$ . The inset shows the same values with a y-axis scaled by an extra polynomial in the logarithm such that linear behavior indicates Gaussian decay structure.

Gaussian states, such as the PPT criterion being both necessary and sufficient for determining separability [127, 137]. In an extension, bi-symmetric  $(\ell \times n)_{\text{mixed}}$  states, in which the  $\ell$  and  $n$  modes exhibit independent permutation symmetries, can be locally transformed into a  $(1 \times 1)_{\text{mixed}}$  state and a set of  $(\ell + n - 2)$  unentangled single modes [134]. Bi-symmetric states thus enjoy the entanglement properties of two-mode Gaussian states [120, 131, 132]. Without local symmetries,  $(\ell \times n)_{\text{pure}}$  Gaussian states can be locally transformed to a set of  $(1 \times 1)_{\text{pure}}$  states and unentangled single modes through local symplectic operations [35, 133]. This is also possible for  $(\ell \times n)_{\text{mixed}}$  isotropic states, which exhibit a global symmetry of constant symplectic eigenvalues (thus a constant multiplicative factor from pure-state covariances) [35]. For  $(\ell \times n)_{\text{mixed}}$  Gaussian states without local or global symmetries, a local unitary has been identified that organizes the inter-region two-body entanglement pairwise [135], though higher-body entanglement through intra-region correlations may remain.

While the lattice vacuum state <sup>3</sup> is not amenable to, or is insufficiently restructured by, the above reorganizations, in the following we demonstrate the existence of a transformation that analogously simplifies its entanglement structure.

### A. Structure of Negativity Core

As described with constructive techniques in the following, the local operators designed to consolidate the entanglement of the  $(d \times d)_{\text{mixed}}$  field regions are informed by the partially transposed (PT) symplectic eigensystem. This is the eigensystem in which additivity is enjoyed by the quantum logarithmic negativity [118–121], which bounds the distillable entanglement by probing the deviation of a quantum state from physicality upon local application of the transposition positive map (see Section S1 for further discussion). It has been observed [51, 53] that the number of PT symplectic eigenvalues contributing to the logarithmic negativity,  $n_-$ , decreases rapidly with the spatial separation between the regions. At large separation near the entanglement sphere boundary where latticized regions become separable [53] and negativity vanishes [34, 35, 38, 39, 42, 45–48, 50, 53, 66], the negativity is characterized by a single ground state mode. At large distances outside the slightly smaller entanglement sphere of  $(d-1 \times d-1)_{\text{mixed}}$  vacuum regions, the distillable entanglement of this single mode becomes maximally delocalized into genuine  $(d \times d)$ -body entanglement, in which all smaller subsets of modes are separable [53]. At reduced field separations, or towards the field continuum, the localized negativity contributions in the PT basis gains exponential tails, subsequently associated with genuine  $(k \times k)$ -body entanglement between the field regions for  $\ell \leq k \leq d$ , with  $\ell$  a lattice-separation-dependent constant that becomes equal to one at zero separation. These features of the PT basis are shown in Fig. S1 for a representative system of pixelated regions of the vacuum.

In light of this structure and PT ground state dominance, it is advantageous to consider the construction of a symplectic operator that localizes the PT ground state mode into a single physical mode of the CV system. By further building the local operator leveraging the PT basis and a symplectic Gram-Schmidt (sGS) procedure (see Section S2 C) to enforce

<sup>3</sup> See Section S1 of Ref. [130] for a Gaussian CV formulation.

unitarity in the Hilbert space, the transformed mode pairs carry the same entanglement hierarchy as the PT negativity contributions (see Section S2D for examples). Subsequently, field negativity can be extracted through  $(1 \times 1)_{\text{mixed-mode}}$  techniques for each of the  $n_c$  core pairs. In particular, it is found that  $n_c = n_-$ , with the negativity contributions mapping one-to-one between core pairs and PT symplectic eigenvalues.

The ability to consolidate (or delocalize through reversal) distillable entanglement in the field through local transforms, from volume-to-volume dispersed calculations plagued by a sign problem [51, 53] to consolidated pairs of additively contributing entangled modes, suggests that both computational and conceptual advantages are possible through a mindful delocalization of lattice degrees of freedom, likely with analogy to the holographic techniques connecting entanglement in conformal fields to geometries in bulk gravitational duals [37, 41, 163]. In particular, the exponential hierarchy of entanglement present in the core mode pairs may provide a non-local scheme for entanglement truncation with systematically quantifiable uncertainties.

### B. Explicit Construction of Local Transformation

Utilizing the framework of Section S1 with  $4d$ -dimensional CMs for a lattice of  $d$  sites in each of two regions, a technique of entanglement consolidation is now described for the regions of the vacuum of lattice scalar field theory. For the matrices of two point correlation functions,

$$G_{i,j} = \langle \phi_i \phi_j \rangle \quad , \quad H_{i,j} = \langle \pi_i \pi_j \rangle \quad , \quad (\text{S12})$$

consider the left and right eigenvectors of  $GH^\Gamma$  calculated as,

$$H^\Gamma G \bar{\mathbf{v}}_{x,j} = \lambda_j^2 \bar{\mathbf{v}}_{x,j} \quad , \quad GH^\Gamma \bar{\mathbf{v}}_{p,j} = \lambda_j^2 \bar{\mathbf{v}}_{p,j} \quad , \quad (\text{S13})$$

where the  $\lambda_j$  are the PT symplectic eigenvalues calculated as the eigenvalues of  $|i\Omega\sigma^\Gamma|$ . While use of this basis organizes the distribution of negativity, one may choose a standard normalization for concreteness to set the first elements positive  $(\bar{\mathbf{v}}_{x,1})_1, (\bar{\mathbf{v}}_{p,1})_1 \geq 0$  and,

$$\bar{\mathbf{v}}_{x,j}^T G \bar{\mathbf{v}}_{x,j} = \lambda_j \quad , \quad \bar{\mathbf{v}}_{p,j}^T H^\Gamma \bar{\mathbf{v}}_{p,j} = \lambda_j \quad , \quad \bar{\mathbf{v}}_x \cdot \bar{\mathbf{v}}_p^T = \mathbb{I} \quad , \quad (\text{S14})$$

where  $\bar{\mathbf{v}}_x, \bar{\mathbf{v}}_p$  without further indices are stacked matrices with rows corresponding to the PT symplectic eigenvectors. Subsequently, a local transformation basis is extracted from this eigenvector set as,

$$\bar{S}_A = \begin{pmatrix} \left( \begin{array}{c} \bar{\mathbf{v}}_{x,1} \\ \bar{\mathbf{v}}_{p,1} \end{array} \right)_A \\ \vdots \\ \left( \begin{array}{c} \bar{\mathbf{v}}_{x,d} \\ \bar{\mathbf{v}}_{p,d} \end{array} \right)_A \end{pmatrix} \quad , \quad (\text{S15})$$

where  $d$  is the number of modes per region of the field and the subscript indicates that the eigenvector has been cut at the dimensionality of the first field region. Importantly, these vectors are not eigenvectors of the  $A$ -region alone that would serve to diagonalize the local region CMs. Note that there are  $2d$  eigenvectors with positive  $\lambda_m$  eigenvalue. In the declared ordering, only the half with the lowest PT symplectic eigenvalues are retained to span the local transformation basis. For any  $(n_a + n_b)$ -mode Gaussian system, the maximum number of negative eigenvalues possibly contributing to the negativity is  $\min(n_a, n_b)$ , the minimum number of modes in either region [137]. As such, the choice of utilizing the lowest  $d$  left and right eigenvectors to initialize a local symplectic transformation captures all available negativity. Note that while entanglement consolidating transformations for pure states can be informed solely through the local CMs [35, 133], this consolidation depends upon full CM diagonalization, consistent with extensions of entanglement quantifications from pure to mixed states.

While offering a transformation between local basis vectors and the Gaussian modes dominantly contributing to the negativity,

$$\{\mathbf{e}_{x,j}, \mathbf{e}_{p,j}\} \xleftrightarrow{S_A} \{(\bar{\mathbf{v}}_{x,j})_A, (\bar{\mathbf{v}}_{p,j})_A\} \quad \forall j \in \{1, \dots, d\} \quad , \quad (\text{S16})$$

the operator as described is not symplectic. To rectify this property, the symplectic Gram-Schmit (sGS) procedure, discussed in Section S2C, is applied to produce a symplectic transformation  $S_A$  in the first region.

The associated transformation in the second region,  $S_B$ , can be determined through symmetry transformation of  $S_A$ , e.g., a reversal of Gaussian mode order for a one-dimensional system. The local, symplectic operator,  $S = S_A \oplus S_B$ , thus

transforms the non-local negativity basis with a clear hierarchy into pairs of local basis vectors, consolidating the distillable entanglement into corresponding pairs of Gaussian modes,

$$\sigma' = S\sigma S^T \quad , \quad S = S_A \oplus S_B \quad . \quad (\text{S17})$$

The locally-transformed  $\sigma'$  exhibits entanglement that manifests the negativity core in the first  $n_c = n_-$  modes in either region.

In order to describe a physical unitary transformation on the Hilbert space, a symplectic operation  $S$  has been determined acting upon the CM. In order for that symplectic operation to generate the hierarchy of negativity contributions observed in the field, the symplectic eigenbasis of the PT CM has been employed in the calculation of  $S$ . While this connection is not generically valid, even for local operations  $S_{arb} = S_{a,A} \oplus S_{a,B}$ , as symplectic operations do not generically commute with the active portion of the partial transposition operator  $[S_{a,B}, Z^\oplus] \neq 0$ , the particular choice of local operation in Eq. (S15) that acts as a separate transformation in the local  $\phi$  and  $\pi$  quadrature bases does allow commutation  $[S, \Gamma] = 0$ . In a system without mixed expectation values ( $\langle \phi_i \pi_j \rangle = 0 \ \forall i, j$ ), a negativity-informed transformation can thus be determined for application on the physical system.

After the above transformation defined by the symplectic eigenvectors, negativity is captured in  $(1_A \times 1_B)_{\text{mixed}}$  pairs of local modes as governed by the PT symplectic eigenvalues,

$$\begin{aligned} \mathcal{N}(\sigma'(1, 2d)) &= \mathcal{N}_1 \quad , \\ \mathcal{N}(\sigma'(2, 2d-1)) &= \mathcal{N}_2 \quad , \\ &\vdots \\ \mathcal{N}(\sigma'(d, d+1)) &= \mathcal{N}_d \quad , \end{aligned} \quad (\text{S18})$$

where  $\sigma'(i, j)$  is the 2-mode reduced CM of  $\sigma'$  with the  $i^{\text{th}}$  and  $j^{\text{th}}$  modes.

Some aspects of this core structure apply to a broader class of mixed CV quantum states. In particular, consider  $D$ -type CMs, which may be decomposed as,

$$\sigma_D = D(n). \Sigma. D^T(n) \quad , \quad (\text{S19})$$

$$D(n) = \begin{pmatrix} C & 0 \\ 0 & C^{-T} \end{pmatrix} \quad , \quad C \in GL(n; \mathbb{R}) \quad , \quad (\text{S20})$$

where  $D(n)$  is one generator of the symplectic group, written in a basis of  $\{x_1, \dots, x_n, p_1, \dots, p_n\}$  and  $\Sigma$  is a diagonal matrix with elements  $\Sigma_i \geq 1$ . This class of mixed CMs share the property of vanishing  $\langle x_i p_j \rangle$  matrix elements, as can be seen by the lack of off-diagonal matrix elements in  $D(n)$ . This condition, as discussed above, allows the PT to commute with the consolidating local transformation calculated with these methods, and thus allows the PT symplectic spectrum to inform entanglement organizing unitaries in the physical space. While not a sufficient condition to organize distillable entanglement into separate  $(1 \times 1)_{\text{mixed}}$  mode pairs as described in Eq. (S18), the first  $k$  pairs capture the logarithmic negativity associated with the first  $k$  symplectic eigenvalues as,

$$\mathcal{N}(\sigma'_D(1, \dots, k, 2n-k+1, \dots, 2n)) = \sum_{j=1}^k \mathcal{N}_j \quad , \quad (\text{S21})$$

with  $\sigma'_D(1, \dots, k, 2n-k+1, \dots, 2n)$  the  $2k$ -mode reduced  $D$ -type CM after application of the negativity consolidating transformation. This accumulative core structure, relevant beyond the lattice scalar field vacuum, arises as a result of the sGS procedure used to generate a valid symplectic transformation for negativity consolidation from the PT symplectic eigenvectors.

### C. Symplectic Gram Schmidt

The symplectic Gram-Schmidt (sGS) aims to produce a set of symplectically orthogonal vectors seeded by an initial basis of interest,  $\{\bar{\mathbf{v}}\}$ . The symplectic inner product is written as,

$$\langle \mathbf{u}, \mathbf{v} \rangle_\Omega = \mathbf{u} \Omega \mathbf{v}^T \quad , \quad (\text{S22})$$

which by symmetry vanishes for the autoprodut of any real vector,  $\langle \mathbf{v}, \mathbf{v} \rangle_\Omega = 0$ . The aim of the sGS procedure is to produce a basis for which  $\langle \mathbf{v}_i, \mathbf{v}_j \rangle_\Omega = \Omega_{i,j}$ . Subsequently constructing an operator,  $S$ , through the stacking of these basis vectors in rows will produce a symplectic transformation preserving the canonical commutation relations,  $S \Omega S^T = \Omega$ , by design.

At each step of the sGS, vectors in the basis must be symplectically orthogonalized and normalized. Consider the first two vectors proposed  $\bar{\mathbf{v}}_{x,1}, \bar{\mathbf{v}}_{p,1}$  corresponding to the two quadratures of the first mode. By symmetry, the diagonal elements of the intended inner product vanish such that only the normalization requires modification,

$$\mathbf{v}_{x,1} = \frac{\bar{\mathbf{v}}_{x,1}}{\sqrt{|\mathcal{A}|}} \quad \mathbf{v}_{p,1} = \frac{\bar{\mathbf{v}}_{p,1}}{\text{sign}(\mathcal{A})\sqrt{|\mathcal{A}|}} \quad \mathcal{A} = \langle \bar{\mathbf{v}}_{x,1}, \bar{\mathbf{v}}_{p,1} \rangle_{\Omega} \quad . \quad (\text{S23})$$

Though alternate distributions of the normalization lead also to effective symplectic transformations for entanglement consolidation, the chosen symmetric distribution between the position and momentum vectors is found to have advantageous properties of numerical stability. For the incorporation of further vectors into the symplectically orthogonal basis, a procedure of removing projective contributions must first be performed,

$$\mathbf{v}'_{z,k} = \bar{\mathbf{v}}_{z,k} - \sum_{j=1}^{k-1} \left[ \langle \mathbf{v}_{x,j}, \bar{\mathbf{v}}_{z,k} \rangle_{\Omega} \langle \mathbf{v}_{x,j}, \mathbf{v}_{p,j} \rangle_{\Omega} \mathbf{v}_{p,j} + \langle \mathbf{v}_{p,j}, \bar{\mathbf{v}}_{z,k} \rangle_{\Omega} \langle \mathbf{v}_{p,j}, \mathbf{v}_{x,j} \rangle_{\Omega} \mathbf{v}_{x,j} \right] \quad , \quad (\text{S24})$$

$$= \bar{\mathbf{v}}_{z,k} - \sum_{j=1}^{k-1} \left[ \langle \mathbf{v}_{x,j}, \bar{\mathbf{v}}_{z,k} \rangle_{\Omega} \mathbf{v}_{p,j} - \langle \mathbf{v}_{p,j}, \bar{\mathbf{v}}_{z,k} \rangle_{\Omega} \mathbf{v}_{x,j} \right] \quad , \quad (\text{S25})$$

with  $z \in \{x, p\}$ , indicating that the symplectic orthogonalization applies equivalently for the position and momentum vectors. The first inner product in each term of Eq. (S24) captures the projection magnitude while the second inner product and vector set the contribution in a direction that will have  $+1$  symplectic overlap with the component being removed. After a final normalization procedure,

$$\mathbf{v}_{x,k} = \frac{\mathbf{v}'_{x,k}}{\sqrt{|\mathcal{A}|}} \quad , \quad \mathbf{v}_{p,k} = \frac{\mathbf{v}'_{p,k}}{\text{sign}(\mathcal{A})\sqrt{|\mathcal{A}|}} \quad , \quad \mathcal{A} = \langle \mathbf{v}'_{x,k}, \mathbf{v}'_{p,k} \rangle_{\Omega} \quad , \quad (\text{S26})$$

the collection of symplectically orthogonal vectors may be organized row-wise to produce a symplectic transformation. For example, in the alternating position-momentum basis described above, the symplectic transformation may be constructed as,

$$S_{i,j} = \begin{cases} \left( \mathbf{v}_{x, \frac{i+1}{2}} \right)_{\frac{j+1}{2}} & i, j \text{ odd} \\ \left( \mathbf{v}_{p, \frac{i}{2}} \right)_{\frac{j}{2}} & i, j \text{ even} \\ 0 & \text{otherwise} \end{cases} \quad . \quad (\text{S27})$$

#### D. Examples: Entanglement Consolidation in the Vacuum

##### 1. $GH^{\Gamma}$ Eigenvectors

Consider the vacuum of one-dimensional massive non-interacting lattice scalar field theory. With two modes per region at zero lattice separation ( $\tilde{r} = 0$ ) and mass arbitrarily chosen to be  $m = 0.003$ , the CM written in the basis of alternating  $\phi$  and  $\pi$  coordinates reads,

$$\sigma = \begin{pmatrix} 2.51 & 0 & 1.87 & 0 & 1.66 & 0 & 1.53 & 0 \\ 0 & 1.27 & 0 & -0.424 & 0 & -0.0849 & 0 & -0.0364 \\ 1.87 & 0 & 2.51 & 0 & 1.87 & 0 & 1.66 & 0 \\ 0 & -0.424 & 0 & 1.27 & 0 & -0.424 & 0 & -0.0849 \\ 1.66 & 0 & 1.87 & 0 & 2.51 & 0 & 1.87 & 0 \\ 0 & -0.0849 & 0 & -0.424 & 0 & 1.27 & 0 & -0.424 \\ 1.53 & 0 & 1.66 & 0 & 1.87 & 0 & 2.51 & 0 \\ 0 & -0.0364 & 0 & -0.0849 & 0 & -0.424 & 0 & 1.27 \end{pmatrix} \quad . \quad (\text{S28})$$

Modes have been ordered from left to right such that the inner two modes correspond to the third through sixth row and column indices. In this alternating basis, the matrix  $G_{i,j} = \langle \phi_i \phi_j \rangle$  of correlation functions is composed of the odd-odd coordinates and the matrix  $H_{i,j} = \langle \pi_i \pi_j \rangle$  is composed of the even-even coordinates of the CM, with a factor of 2 as shown in Eq. (S1). There is one symplectic eigenvalue contributing to the negativity for a total negativity between the two regions of  $\mathcal{N} = 0.654$ . Before and after symplectic orthogonalization, the local transformation is determined by the left and right

eigenvectors of the product  $GH^\Gamma$  as,

$$\bar{S}_A = \begin{pmatrix} 0.0607 & 0 & 0.683 & 0 \\ 0 & 0.321 & 0 & 0.704 \\ 0.762 & 0 & -0.347 & 0 \\ 0 & 0.631 & 0 & -0.0560 \end{pmatrix}, \quad S_A = \begin{pmatrix} 0.0858 & 0 & 0.965 & 0 \\ 0 & 0.454 & 0 & 0.995 \\ 1.08 & 0 & -0.491 & 0 \\ 0 & 0.892 & 0 & -0.0793 \end{pmatrix}. \quad (S29)$$

The transformed CM,

$$\sigma' = S\sigma S^T = \begin{pmatrix} 2.67 & 0 & 0.912 & 0 & 0.912 & 0 & 2.03 & 0 \\ 0 & 1.14 & 0 & 0.0536 & 0 & -0.0536 & 0 & -0.505 \\ 0.912 & 0 & 1.54 & 0 & 0.474 & 0 & 0.912 & 0 \\ 0 & 0.0536 & 0 & 1.08 & 0 & -0.0196 & 0 & -0.0536 \\ 0.912 & 0 & 0.474 & 0 & 1.54 & 0 & 0.912 & 0 \\ 0 & -0.0536 & 0 & -0.0196 & 0 & 1.08 & 0 & 0.0536 \\ 2.03 & 0 & 0.912 & 0 & 0.912 & 0 & 2.67 & 0 \\ 0 & -0.505 & 0 & -0.0536 & 0 & 0.0536 & 0 & 1.14 \end{pmatrix}, \quad (S30)$$

while not visually exhibiting special entanglement structure, captures the negativity core. The negativity that had been distributed nonlocally within the  $(2 \times 2)_{\text{mixed}}$  CM is now localized to the  $(1 \times 1)_{\text{mixed}}$  mode pair of the outer two modes. More precisely, the negativity present in the reduced CM of the first and fourth mode (one from each local region), is equal to the negativity of the full system  $\mathcal{N} = 0.654$ . Though it does not visually appear to be so, an application of separability flow developed in Ref. [146] determines that the  $(1 \times 1)_{\text{mixed}}$  pair of outer modes 1 and 4 is separable from the remaining  $(1 \times 1)_{\text{mixed}}$  pair of inner modes 2 and 3.

While for two lattice sites per region there is only one PT symplectic eigenvalue contributing to the negativity, one can find a set of additive negativity contributions as the pixelation of each region is increased. For example, the same system at zero separation ( $\tilde{r} = 0$ ) and mass ( $m = 0.003$ ) but with four modes per region exhibits three separate contributions to the negativity: 0.858, 0.0230, 0.000298 for a total of  $\mathcal{N} = 0.888$ . The local symplectic transformation designed to localize this negativity into a core of local modes is,

$$S_A = \begin{pmatrix} 0.0286 & 0 & -0.0736 & 0 & -0.190 & 0 & -0.818 & 0 \\ 0 & -0.244 & 0 & -0.460 & 0 & -0.693 & 0 & -1.03 \\ 0.373 & 0 & -0.433 & 0 & -0.803 & 0 & 0.645 & 0 \\ 0 & 0.0505 & 0 & -0.559 & 0 & -0.741 & 0 & 0.224 \\ 0.386 & 0 & -1.03 & 0 & 0.759 & 0 & -0.143 & 0 \\ 0 & 0.112 & 0 & -0.646 & 0 & 0.379 & 0 & -0.0260 \\ 0.984 & 0 & 0.124 & 0 & -0.0943 & 0 & -0.225 & 0 \\ 0 & 0.960 & 0 & 0.479 & 0 & 0.152 & 0 & -0.0448 \end{pmatrix}. \quad (S31)$$

After this transformation, the pair of outer modes in each region carries an amount of negativity equal to that of the dominant contribution,  $\mathcal{N}_{1,8} = 0.858$ . The second  $(1 \times 1)_{\text{mixed}}$  pair of modes 2 and 7 carry negativity equal to that of the following symplectic eigenvalue,  $\mathcal{N}_{2,7} = 0.0230$ . The remaining pairs continue this pattern governed by the symplectic eigenvalue contributions,  $\mathcal{N}_{3,6} = 0.000298$  and  $\mathcal{N}_{4,5} = 0$ . As the separation between the regions is increased, the number of negativity contributions rapidly diminishes and becomes dominated by a single eigenvalue before vanishing completely. By calculating the local symplectic transformations in this manner, the consolidation of entanglement mimics the structure of symplectic eigenvalues contributing to the negativity.

## 2. $i\Omega\sigma^\Gamma$ Eigenvectors

Above, the local symplectic operators designed to consolidate the vacuum entanglement into a core was informed by the left and right eigenvectors of  $GH^\Gamma$ . Naturally, such a transformation may also be designed from symplectic eigenvectors themselves. Consider the right eigenvectors of the product  $\Omega\sigma^\Gamma\bar{\mathbf{v}}_j = \lambda_j\bar{\mathbf{v}}_j$ . The eigenvalues,  $\lambda_j$ , are the PT symplectic eigenvalues from which the logarithmic negativity may be calculated additively,

$$\mathcal{N} = \sum_{j=1}^{2d} \mathcal{N}_j, \quad \mathcal{N}_j = -\log_2 [\min(|\lambda_j|, 1)]. \quad (S32)$$

Note that the symplectic eigenvalues appear in  $\pm$  pairs through this method of calculation, though do not contribute twice to the negativity. The eigenvectors with paired eigenvalues are related by a conjugation, if  $\lambda_j = -\lambda_k$  then  $\bar{\mathbf{v}}_j = \bar{\mathbf{v}}_k^*$ , up to arbitrary global phases. If ordered from smallest to largest, ignoring  $\bar{\mathbf{v}}_j$  for which  $\lambda_j < 0$ , the initial basis of the local

consolidating symplectic transformation can be chosen as,

$$\bar{S}_A = \begin{pmatrix} \left( \begin{array}{c} \text{Re}\bar{\mathbf{v}}_1 \\ \text{Im}\bar{\mathbf{v}}_1 \end{array} \right)_A \\ \vdots \\ \left( \begin{array}{c} \text{Re}\bar{\mathbf{v}}_d \\ \text{Im}\bar{\mathbf{v}}_d \end{array} \right)_A \end{pmatrix} . \quad (\text{S33})$$

Separating the independent real and imaginary components of each symplectic eigenvector into two basis vectors of the CM informs the two quadratures of each Gaussian mode <sup>4</sup>. In the desired transformation, the eigenvectors  $\bar{\mathbf{v}}_j$  have been each globally phased so that their first elements are real, allowing the resulting symplectic transformation to act separately on the  $(\phi, \pi)$  quadratures without mixture. This separation provides commutation with the PT operation, and thus allows the negativity information in the PT space to be utilized in defining a realizable symplectic transformation on the physical CM, as discussed above. For the purposes of locally transforming two regions of the scalar vacuum into a basis with a manifest negativity core, this choice of information distribution is not unique, e.g., a choice of  $\text{Re}\bar{\mathbf{v}}_1 \pm \text{Im}\bar{\mathbf{v}}_1$  would have a similar effect. The source of arbitrariness in this distribution reflects the arbitrary set of single mode transformations that do not affect the negativity structure of the final CM. After an application of the symplectic Gram-Schmit procedure, the symplectic operator generated from this basis acts upon the CM,  $\sigma' = S\sigma S^T$  with  $S = S_A \oplus S_B$ , and consolidates the entanglement between regions of the field into a number of  $(1 \times 1)_{\text{mixed}}$  mode pairs equal to the number of PT symplectic eigenvalues less than unity, contributing positively to the negativity.

Consider the example of Section S2D1 with two modes per region at zero separation ( $\tilde{r} = 0$ ) and mass of  $m = 0.003$ . The CM written in the basis of alternating  $\phi$  and  $\pi$  coordinates is provided in Eq. (S28). Before and after symplectic orthogonalization, the local transformation is determined by the eigenvectors of the product  $i\Omega\sigma^\Gamma$  as,

$$\bar{S}_A = \begin{pmatrix} 0.041 & 0 & 0.467 & 0 \\ 0 & -0.220 & 0 & -0.482 \\ 0.513 & 0 & -0.234 & 0 \\ 0 & -0.425 & 0 & 0.038 \end{pmatrix} , \quad S_A = \begin{pmatrix} 0.086 & 0 & 0.965 & 0 \\ 0 & 0.454 & 0 & 0.995 \\ 1.077 & 0 & -0.491 & 0 \\ 0 & 0.892 & 0 & -0.079 \end{pmatrix} , \quad (\text{S34})$$

The CM transformed by local consolidating symplectic operation,  $S = S_A \oplus S_B$ , becomes,

$$\sigma' = S\sigma S^T = \begin{pmatrix} 2.670 & 0 & 0.912 & 0 & 0.912 & 0 & 2.034 & 0 \\ 0 & 1.140 & 0 & 0.054 & 0 & -0.054 & 0 & -0.505 \\ 0.912 & 0 & 1.536 & 0 & 0.474 & 0 & 0.912 & 0 \\ 0 & 0.054 & 0 & 1.081 & 0 & -0.020 & 0 & -0.054 \\ 0.912 & 0 & 0.474 & 0 & 1.536 & 0 & 0.912 & 0 \\ 0 & -0.054 & 0 & -0.020 & 0 & 1.081 & 0 & 0.054 \\ 2.034 & 0 & 0.912 & 0 & 0.912 & 0 & 2.670 & 0 \\ 0 & -0.505 & 0 & -0.054 & 0 & 0.054 & 0 & 1.140 \end{pmatrix} . \quad (\text{S35})$$

The negativity that had been distributed nonlocally within the  $(2 \times 2)_{\text{mixed}}$  is again localized to the  $(1 \times 1)_{\text{mixed}}$  mode pair of the outer two modes.

### S3. THE GAUSSIAN SEPARABILITY CRITERION

A necessary and sufficient condition for a Gaussian state,  $\sigma$ , to be separable is the existence of two valid CMs,  $\sigma_a, \sigma_b$  such that [127],

$$\sigma \geq \sigma_a \oplus \sigma_b , \quad \sigma_{a,b} \geq i\Omega . \quad (\text{S36})$$

Physically, this condition can be understood as identifying a valid underlying separable state capable of describing the Gaussian state upon the addition of a PSD matrix characterizing classical noise contributions (perhaps describing classically correlated displacements of the first moments within the ensemble). Reference [146] describes not only how to numerically identify separability/inseparability for mixed Gaussian states, but also provides a constructive method for calculating a

---

<sup>4</sup> Note that this basis is distinct from that utilized by Ref. [122] to demonstrate that non-zero negativity can always be coaxed into a  $(1 \times 1)$ -mode subsystem through local symplectic operations, and thus any NPT entangled Gaussian state provides non-zero distillable entanglement. In particular, the eigenvectors chosen to seed this transformation to the negativity core satisfies  $\bar{\mathbf{v}}^\dagger (\sigma - i\Omega^\Gamma) \bar{\mathbf{v}} \geq 0$ .

viable tensor-product state and classical noise contribution if separability is determined. Applied to the core-halo separability, these techniques identify an explicit decomposition in the form of Eq. 3. For a transformed CM,  $\sigma'$ , in a basis ordered as core modes followed by halo modes,

$$\sigma' = \begin{pmatrix} \sigma'_{cc} & \sigma'_{ch} \\ (\sigma'_{ch})^T & \sigma'_{hh} \end{pmatrix} \quad , \quad (S37)$$

the flow of Ref. [146] begins with the creation of a symmetric object (of modified dimension if the core and halo have different numbers of modes,  $\dim(\sigma'_{cc}) \neq \dim(\sigma'_{hh})$ ) as,

$$\sigma'_1 = \begin{pmatrix} \sigma'_{cc} - \text{Re}(X) & -\text{Im}(X) \\ -\text{Im}(X^T) & \sigma'_{cc} - \text{Re}(X) \end{pmatrix} \quad , \quad (S38)$$

with  $X = \sigma'_{ch} (\sigma'_{hh} - i\Omega)^{-1} (\sigma'_{ch})^T$ . This transformation describes a flow,  $\sigma'_k$  for increasing  $k$ , that can be iterated until separability/inseparability is determined. After the first step (and generalized to further steps if necessary), the condition for separability is

$$\sigma_c = \sigma'_{cc} - \text{Re}(X) - \|\text{Im}(X)\|_{op} \mathbb{I} \geq i\Omega \quad , \quad (S39)$$

where the operator norm  $\|\xi\|_{op}$  is the maximum eigenvalue of  $\sqrt{\xi^\dagger \xi}$ . This condition means that separability between the core and halo is identified if  $\sigma_c$  is a valid CM. A constructive relationship is then found to be,

$$\sigma'_1 = \sigma_c \otimes \sigma_c + Y_1 \quad , \quad (S40)$$

where  $Y_1$  is a PSD matrix and thus a valid characterization of classical noise. This information can be transferred back through the flow to inform a decomposition of the physical  $\sigma'$  as,

$$\sigma' = \sigma_c \oplus \sigma_h + Y \quad , \quad \sigma_h = \sigma'_{hh} - (\sigma'_{ch})^T (\sigma'_{cc} - \sigma_c)^{-1} \sigma'_{ch} \quad , \quad (S41)$$

where again  $Y$  is a PSD matrix. When  $(\sigma'_{cc} - \sigma_c)$  is singular, as is often the case in the scalar field vacuum, the pseudoinverse can be utilized for successful identification of a valid tensor-product and noise decomposition. However, the associated poor condition numbers often require high precision (hundreds of digits for applications in the main text) to maintain numerical stability. Conveniently, the core-halo separability of the field is observed to be determined after a single step in the flow, and thus  $\sigma'_k$  for  $k = 1$  is sufficient for quantifying the SOE of Fig. 2. For constructive decompositions at higher flow depth, an additional step of symmetrization is required as separable states underlying the noise are tracked backwards through the flow to the original physical CM. Reference [146] provides further details.

The following is an example of sequentially applying this separability criterion to establish simultaneous separability among the core pairs. If the number of core mode pairs (and thus the number of symplectic eigenvalues),  $n_c$ , is four, one possible two-level splitting procedure that may yield a fully separable pair decomposition in the core is,

$$\begin{aligned} \sigma_c &= \sigma_{c,12} \oplus \sigma_{c,34} + Y_1 \quad , \\ \sigma_{c,12} &= \sigma_{c,1} \oplus \sigma_{c,2} + Y_2 \quad , \\ \sigma_{c,34} &= \sigma_{c,3} \oplus \sigma_{c,4} + Y_3 \quad , \end{aligned} \quad (S42)$$

where the  $Y_i$  are all PSD matrices representing additional local noise contributions. With such sequential bipartitions, the simultaneous separability of the core would be identified as,

$$\sigma' = \sigma_{c,1} \oplus \sigma_{c,2} \oplus \sigma_{c,3} \oplus \sigma_{c,4} \oplus \sigma_h + Y + \sum_i Y_i \quad , \quad (S43)$$

where the  $Y_i$ 's are understood to be placed in their relevant Hilbert spaces completed by **0** block matrices. For  $n_c = 2$ , this sequential procedure is achieved in one level with no ambiguity. For  $n_c > 2$ , this sequential procedure requires multiple levels with an array of different possible splitting structures at each level. Though not all sequences allow identification of Eq. (7) structure (indicating incompatible noise assignments for subsequent levels), a simple search over multiple splitting sequences allows full simultaneous separability in the core to be reliably identified. The rapid loss of numerical precision through this technique with matrix inversions at each level demands utilization of arbitrary precision libraries with several hundreds of digits to calculate the simultaneously separable decomposition of Eq. (7), exacerbated for fixed  $n_c$  at large number of lattice sites per region,  $d$ , and associated spatial separations.

#### S4. SEPARABILITY-OBSCURED ENTANGLEMENT (SOE)

For mixed states, the designation of Hilbert space separability expresses the existence of a convex density matrix decomposition of only tensor-product pure states,

$$\rho_{\text{separable}} = \sum_i p_i \rho_i^A \otimes \rho_i^B \quad , \quad (\text{S44})$$

with positive, real weights  $\sum_i p_i = 1$ . However, it is possible for both tensor-product and entangled convex decompositions to exist as compatible underlying descriptions of a separable mixed-state density matrix. For a concrete two qubit example in which a separable state can be produced with distributed entanglement, consider the mixture of a Bell state with the maximally mixed state,

$$\rho(\eta) = \eta \rho \left( \frac{|00\rangle + |11\rangle}{\sqrt{2}} \right) + (1 - \eta) \frac{\mathbb{I}}{4} \quad , \quad (\text{S45})$$

known as an isotropic state or two-qubit Werner state up to local transformation [164, 165]. In two-qubit systems, negativity is both necessary and sufficient for the identification of separability. With this quantity, it can be determined that the mixture in Eq. (S45) is separable (i.e., compatible with a mixture of unentangled states) in the regime  $\eta \leq 1/3$ . Explicitly, one viable tensor-product decomposition of this density matrix is,

$$\begin{aligned} \rho(\eta) = & \frac{\eta}{2} [\rho(|++\rangle_x) + \rho(|--\rangle_x) + \rho(|+-\rangle_y) + \rho(|-+\rangle_y)] \\ & + \frac{1-\eta}{4} [\rho(|00\rangle) + \rho(|11\rangle)] + \frac{1-3\eta}{4} [\rho(|01\rangle) + \rho(|10\rangle)] \quad , \end{aligned} \quad (\text{S46})$$

where  $\rho(|\psi\rangle) = |\psi\rangle\langle\psi|$  is the density matrix associated with pure state  $|\psi\rangle$ ,  $|\pm\rangle_x = \frac{|0\rangle \pm |1\rangle}{\sqrt{2}}$ , and  $|\pm\rangle_y = \frac{|0\rangle \pm i|1\rangle}{\sqrt{2}}$ . This decomposition is convex only for  $\eta \leq 1/3$ , beyond which the state is entangled and the last coefficient becomes negative <sup>5</sup>. Thus, it is possible that the regime identified as separable can be physically produced through Eq. (S46) with solely classical correlations or through Eq. (S45) as a mixed ensemble of entangled pairs and unentangled basis states, dominated by the latter.

Two parties, A and B, receiving distributed samples of this separable state ( $\eta \leq 1/3$ ) from a source will not be able to distinguish between the entangled and unentangled production mechanisms, even with classical communication and a complete tomography of the mixed density matrix that they share. However, with the addition of classical communication from the source to parties A and B, e.g., indexing the pure state from which each provided sample was generated as in Eq. (S45), parties A,B may be able to extract entangled pairs. For states with SOE, it is possible to identify distributed entanglement provided only additional classical communication from the source. This is a physical mechanism underlying observations of “hidden”, “unlockable”, and “non-robust” entanglement [138–141] and non-classical correlations in separable mixed states, quantified, for example, by the quantum discord and identified to be abundant in the Hilbert space [166–168]. The presence of quantum correlations in separable density matrices with non-zero quantum discord is dependent upon the explicit convex decomposition utilized to prepare the state.

Though not accessible with only access to the density matrix, the convex decomposition employed in the creation of a mixed quantum state is a physical characteristic relevant to experimental preparation procedures, and thus relevant to the physical presence of distributed entanglement. While the generation of separable state density matrices can always be achieved without entanglement, they may also be generated through entangled convex combinations. Depending upon experimental processes, formally separable states can obscure entanglement and thus, with strategically designed classical information from the source, be useful resources for quantum information purposes.

##### A. Example: SOE in the Lattice Scalar Field Vacuum

The following is an explicit example of a mixed state of four CV quantum modes, transformed from a pair of low-pixelation vacuum regions, that exhibits both core-halo and  $\text{halo}_A$ - $\text{halo}_B$  separability but is not simultaneously separable along these two partitions. In particular, despite this pair of separability observations, the distillable entanglement between, for example,  $\text{halo}_A$  and the rest of the system, will be non-zero. Compilation of these observations, and their higher-pixelation counterparts, will indicate the presence of SOE between scalar vacuum regions.

<sup>5</sup> This decomposition further provides a simple example of how observables within inseparable states may be informed by stochastic application of unentangled ensembles, at the cost of systematically exacerbated sign problems as a function of separability violation or entanglement.

Consider the CM associated with two sites per region, shown in Eq. (S30). Having been transformed through local symplectics, modes 1 and 4 comprise  $\text{core}_A$  and  $\text{core}_B$ , while modes 2 and 3 comprise  $\text{halo}_A$  and  $\text{halo}_B$ , where  $A, B$  indicates the associated region of the scalar field vacuum. Through the techniques described in Ref. [146], core-halo separability is identified through the inequality of Eq. (3) with the following decomposition,

$$\sigma_c = \begin{pmatrix} 1.1143 & 0 & 0.4785 & 0 \\ 0 & 1.1044 & 0 & -0.4687 \\ 0.4785 & 0 & 1.1143 & 0 \\ 0 & -0.4687 & 0 & 1.1044 \end{pmatrix}, \quad \sigma_h = \begin{pmatrix} 1.0018 & 0 & -0.0600 & 0 \\ 0 & 1.0018 & 0 & 0.0600 \\ -0.0600 & 0 & 1.0018 & 0 \\ 0 & 0.0600 & 0 & 1.0018 \end{pmatrix}, \quad (S47)$$

$$Y = \begin{pmatrix} 1.5553 & 0 & 1.5553 & 0 & 0.9115 & 0 & 0.9115 & 0 \\ 0 & 0.0360 & 0 & -0.0360 & 0 & 0.0536 & 0 & -0.0536 \\ 1.5553 & 0 & 1.5553 & 0 & 0.9115 & 0 & 0.9115 & 0 \\ 0 & -0.0360 & 0 & 0.0360 & 0 & -0.0536 & 0 & 0.0536 \\ 0.9115 & 0 & 0.9115 & 0 & 0.5343 & 0 & 0.5343 & 0 \\ 0 & 0.0536 & 0 & -0.0536 & 0 & 0.0796 & 0 & -0.0796 \\ 0.9115 & 0 & 0.9115 & 0 & 0.5343 & 0 & 0.5343 & 0 \\ 0 & -0.0536 & 0 & 0.0536 & 0 & -0.0796 & 0 & 0.0796 \end{pmatrix}, \quad (S48)$$

in the basis of  $\{\text{core}_A, \text{core}_B, \text{halo}_A, \text{halo}_B\}$ .

For Gaussian states with density matrix  $\rho$ , the purity may be calculated from the associated CM,  $\sigma$ , as  $\text{Tr}(\rho^2) = 1/\sqrt{\det(\sigma)}$ . A decomposition with  $\sigma_c$  and  $\sigma_h$  pure can always be created as mixed Gaussian states may be described as randomly displaced pure states. One method for separating the pure contribution is to utilize the Williamson normal decomposition in which a CM is diagonalized through global symplectic operations,  $\sigma = S_W \Sigma S_W^T$ , where  $\Sigma$  is diagonal and  $S_W$  is symplectic. After identification of the symplectic operation that transforms to the Williamson normal form, the CM can be separated into a pure state (with  $\Sigma = \mathbb{I}$ ) and a PSD noise contribution describing classically distributed displacements,

$$\sigma = S_W S_W^T + S_W (\Sigma - \mathbb{I}) S_W^T = \sigma^{(p)} + Y^{(p)} . \quad (S49)$$

When applied to the core-halo decomposition,

$$\begin{aligned} \sigma' = \sigma_c \oplus \sigma_h + Y &= \sigma_c^{(p)} \oplus \sigma_h^{(p)} + Y_c^{(p)} \oplus Y_h^{(p)} + Y \\ &= \sigma_c^{(p)} \oplus \sigma_h^{(p)} + Y^{(p)} , \end{aligned} \quad (S50)$$

the explicit CM and noise matrices become,

$$\sigma_c^{(p)} = \begin{pmatrix} 1.1093 & 0 & 0.4736 & 0 \\ 0 & 1.1024 & 0 & -0.4706 \\ 0.4736 & 0 & 1.1093 & 0 \\ 0 & -0.4706 & 0 & 1.1024 \end{pmatrix}, \quad \sigma_h^{(p)} = \begin{pmatrix} 1.0018 & 0 & -0.0600 & 0 \\ 0 & 1.0018 & 0 & 0.0600 \\ -0.0600 & 0 & 1.0018 & 0 \\ 0 & 0.0600 & 0 & 1.0018 \end{pmatrix}, \quad (S51)$$

$$Y^{(p)} = \begin{pmatrix} 1.5602 & 0 & 1.5602 & 0 & 0.9115 & 0 & 0.9115 & 0 \\ 0 & 0.0381 & 0 & -0.0341 & 0 & 0.0536 & 0 & -0.0536 \\ 1.5602 & 0 & 1.5602 & 0 & 0.9115 & 0 & 0.9115 & 0 \\ 0 & -0.0341 & 0 & 0.0381 & 0 & -0.0536 & 0 & 0.0536 \\ 0.9115 & 0 & 0.9115 & 0 & 0.5343 & 0 & 0.5343 & 0 \\ 0 & 0.0536 & 0 & -0.0536 & 0 & 0.0796 & 0 & -0.0796 \\ 0.9115 & 0 & 0.9115 & 0 & 0.5343 & 0 & 0.5343 & 0 \\ 0 & -0.0536 & 0 & 0.0536 & 0 & -0.0796 & 0 & 0.0796 \end{pmatrix} . \quad (S52)$$

Written in this form, a preparation procedure can be imagined for two-site pixelated regions of the vacuum through distribution of two two-mode pure entangled CV states,  $\sigma_{c,h}$ , and the addition of classical noise. The added noise causes  $\sigma_h$  to exhibit only SOE, and thus the distillable entanglement of the second pair to vanish.

The shaded sub-blocks in the noise matrices indicate  $\delta$  of Eq. (3), where the PSD property after replacement of  $\delta$  by the noise structure of halo separability,  $Y_h$ , will determine whether the core-halo and  $\text{halo}_A$ - $\text{halo}_B$  can be simultaneously separable. Similar techniques to those above allow the  $\text{halo}_A$ - $\text{halo}_B$  separability to be identified through the inequality of Eq. (4) with the following decomposition,

$$\sigma_{h,A}^{(p)} = \sigma_{h,B}^{(p)} = \begin{pmatrix} 0.9951 & 0 \\ 0 & 1.0050 \end{pmatrix}, \quad Y_h^{(p)} = \begin{pmatrix} 0.5410 & 0 & 0.4743 & 0 \\ 0 & 0.0765 & 0 & -0.0196 \\ 0.4743 & 0 & 0.5410 & 0 \\ 0 & -0.0196 & 0 & 0.0765 \end{pmatrix} . \quad (S53)$$

For clarity, a symmetric decomposition with  $\sigma_{h,A}^{(p)} = \sigma_{h,B}^{(p)}$  has been chosen. The simultaneous separability condition may be explored through replacement of the lower block of  $Y$  with  $Y_h$ , creating  $Y'$  as discussed in Eq. 6. The resulting absence of PSD structure (negative  $Y'$ -eigenvalues of  $-0.037$  and  $-0.024$ ) indicates that these particular separability observations

are not simultaneously realizable. Furthermore, this lack of simultaneity is decisively confirmed in the presence of non-zero negativity (and thus the presence of distillable entanglement) between  $\text{halo}_A$  and the rest of the system  $\mathcal{N}_{\text{halo}_A|\text{halo}_B,\text{core}} = 0.022$ . Note that this incompatibility is also heralded by  $\sigma_h$  alone, which is found to exhibit negativity  $\mathcal{N}_{A,B}(\sigma_h) = 0.087$  and therefore is inseparable, indicating the presence of SOE within the halo subsystem and thus BE within the full NPT state<sup>6</sup>.

## B. Separability-Obscured Entanglement and Bound Entanglement

In this paper, we conjecture that SOE provides a physical interpretation of BE. If this picture is encompassing,  $\text{BE} \subset \text{SOE}$ , then established systems exhibiting BE must be interpretable as distillable states that have become compatible with a separable description through the presence of classical noise.

In a first demonstration of BE in CV systems, the following  $(2 \times 2)_{\text{mixed}}$  integer-element CM was provided as a concrete example of BE in Ref. [127],

$$\sigma_{BE} = \begin{pmatrix} 2 & 0 & 0 & 0 & 1 & 0 & 0 & 0 \\ 0 & 1 & 0 & 0 & 0 & 0 & 0 & -1 \\ 0 & 0 & 2 & 0 & 0 & 0 & -1 & 0 \\ 0 & 0 & 0 & 1 & 0 & -1 & 0 & 0 \\ 1 & 0 & 0 & 0 & 2 & 0 & 0 & 0 \\ 0 & 0 & 0 & -1 & 0 & 4 & 0 & 0 \\ 0 & 0 & -1 & 0 & 0 & 0 & 2 & 0 \\ 0 & -1 & 0 & 0 & 0 & 0 & 0 & 4 \end{pmatrix} . \quad (\text{S54})$$

The negativity between the first two (A) and last two (B) modes vanishes,  $\mathcal{N}_{A|B}(\sigma_{BE}) = 0$ , indicating zero distillable entanglement. Additionally, application of the CV separability criterion [127] indicates, in two steps of the flow [146], that the system is inseparable across the A,B two-mode partition. This pair of observations conclusively identifies the presence of PPT bound entanglement.

To reveal a physical description of this BE, two further separability observations are of interest. First, all  $(1_A \times 1_B)_{\text{mixed}}$  pairs spanning the partition are found to be separable upon tracing of the remaining two modes. Second, these pairs are separable from each other<sup>7</sup>, i.e., the  $(2 \times 2)_{\text{mixed}}$  state can be regarded as a set of two  $(1_A \times 1_B)_{\text{mixed}}$  BE states. Applying techniques of Ref. [146], discussed in the main text for identification of explicit core-halo decompositions, physical representations of  $\sigma_{BE}$  can be found that reveal distillably entangled states spanning the A,B spaces upon classical noise removal. Consider the separability identification between  $(1_A \times 1_B)_{\text{mixed}}$  modes in the configuration of (1,4) and (2,3). The CM may be decomposed as,

$$\sigma_{BE}^{(1,4,2,3)} = \begin{pmatrix} 2 & 0 & 0 & 0 & 0 & 0 & 1 & 0 \\ 0 & 1 & 0 & -1 & 0 & 0 & 0 & 0 \\ 0 & 0 & 2 & 0 & -1 & 0 & 0 & 0 \\ 0 & -1 & 0 & 4 & 0 & 0 & 0 & 0 \\ 0 & 0 & -1 & 0 & 2 & 0 & 0 & 0 \\ 0 & 0 & 0 & 0 & 0 & 1 & 0 & -1 \\ 1 & 0 & 0 & 0 & 0 & 0 & 2 & 0 \\ 0 & 0 & 0 & 0 & 0 & -1 & 0 & 4 \end{pmatrix} = \sigma_{14} \oplus \sigma_{23} + Y , \quad (\text{S55})$$

with

$$\sigma_{14} = \sigma_{23} = \begin{pmatrix} \frac{4}{3} & 0 & \frac{1}{3} & 0 \\ 0 & 1 & 0 & -1 \\ \frac{1}{3} & 0 & \frac{1}{3} & 0 \\ 0 & -1 & 0 & 4 \end{pmatrix} , \quad Y = \begin{pmatrix} \frac{2}{3} & 0 & -\frac{1}{3} & 0 & 0 & 0 & 1 & 0 \\ 0 & 0 & 0 & 0 & 0 & 0 & 0 & 0 \\ -\frac{1}{3} & 0 & \frac{5}{3} & 0 & -1 & 0 & 0 & 0 \\ 0 & 0 & 0 & 0 & 0 & 0 & 0 & 0 \\ 0 & 0 & -1 & 0 & \frac{2}{3} & 0 & -\frac{1}{3} & 0 \\ 0 & 0 & 0 & 0 & 0 & 0 & 0 & 0 \\ 1 & 0 & 0 & 0 & -\frac{1}{3} & 0 & \frac{5}{3} & 0 \\ 0 & 0 & 0 & 0 & 0 & 0 & 0 & 0 \end{pmatrix} . \quad (\text{S56})$$

<sup>6</sup> Note that the terminology of BE continues to evolve. For example, the conclusion of NPT distillability in Ref. [122] was contextualized as showing that there does not exist NPT BE Gaussian states. In that application, the language of BE was utilized in the binary sense of complete indistillability. As discussed in the main text, we utilize the broader definition of BE [123] as the operational difference between the entanglement utilized to create a state and the entanglement that can be subsequently extracted.

<sup>7</sup> For clarity, (1,4) is separable from (2,3) and (1,3) is separable from (2,4).

This decomposition suggests a viable state preparation mechanism consisting of two distributed  $(1 \times 1)_{\text{mixed}}$  states (which may be purified as discussed in Eq. (S49)) convolved with classically correlated Gaussian noise in the position coordinates of phase space. The bona fide CMs of the distributed pairs,  $\sigma_{14}$  and  $\sigma_{23}$ , exhibit non-zero negativity with  $\mathcal{N}_{A|B}(\sigma_{14}) = \mathcal{N}_{A|B}(\sigma_{23}) = \frac{\log(3)}{2\log(2)}$ . This situation is directly analogous to that discussed in the main text for core-halo non-simultaneous separability leading to subsystem SOE, this time in halo-halo form. In contrast to the lattice scalar field vacuum, this example shows that a  $(2 \times 2)_{\text{mixed}}$  PPT BE state can be decomposed into a pair of  $(1 \times 1)_{\text{mixed}}$  states each with distillable entanglement and classical noise. With this representation, it is clear that one physical explanation for the presence of BE in this system is that classical noise has caused the underlying states with distillable entanglement to become compatible with a separable description.

## S5. NUMERICAL TABLES

In this section we provide numerical values appearing main text figures. Table S1 corresponds to Fig. S1 presenting the logarithmic negativity contributions organized by PT symplectic eigenvalues for a variety of region separations in the vacuum. Tables S2-S4 correspond to Fig. 2 presenting the region-region logarithmic negativity,  $\mathcal{N}_{A|B}(\sigma)$ , and the bound logarithmic negativity between regions in the halo,  $\mathcal{N}_{A|B}(\sigma_h)$  for  $d = 10, 20$ . Further numerical values are available upon request.

$\tilde{r}$	$\mathcal{N}_j$								
	1.360								
	$2.143 \times 10^{-1}$		$1.857 \times 10^{-1}$		$9.067 \times 10^{-2}$		$3.295 \times 10^{-2}$		$4.314 \times 10^{-3}$
	$2.775 \times 10^{-2}$		$5.312 \times 10^{-3}$		$1.204 \times 10^{-3}$		$4.939 \times 10^{-6}$		$1.538 \times 10^{-7}$
	$2.650 \times 10^{-3}$		$1.761 \times 10^{-4}$		$4.399 \times 10^{-8}$		$3.902 \times 10^{-5}$		$5.242 \times 10^{-12}$
	$2.117 \times 10^{-4}$		$4.880 \times 10^{-6}$		$2.799 \times 10^{-8}$		$4.473 \times 10^{-11}$		$9.355 \times 10^{-17}$
	$1.252 \times 10^{-5}$		$7.475 \times 10^{-8}$		$5.584 \times 10^{-13}$		$1.319 \times 10^{-14}$		$1.350 \times 10^{-21}$
	$6.810 \times 10^{-7}$		$4.128 \times 10^{-10}$		$3.079 \times 10^{-15}$		$1.971 \times 10^{-17}$		$3.085 \times 10^{-27}$
	$2.581 \times 10^{-8}$		$5.458 \times 10^{-12}$		$1.580 \times 10^{-17}$		$1.976 \times 10^{-21}$		$5.506 \times 10^{-33}$
0	$9.840 \times 10^{-10}$	5	$6.857 \times 10^{-14}$	10	$8.574 \times 10^{-18}$	20	$1.220 \times 10^{-19}$	40	$7.941 \times 10^{-38}$
	$2.352 \times 10^{-11}$		$1.055 \times 10^{-15}$		$1.017 \times 10^{-19}$		$4.124 \times 10^{-22}$		$6.551 \times 10^{-4}$
	$6.284 \times 10^{-13}$		$1.580 \times 10^{-17}$		$4.554 \times 10^{-22}$		$7.510 \times 10^{-25}$		$6.670 \times 10^{-10}$
	$9.023 \times 10^{-15}$		$8.574 \times 10^{-18}$		$3.610 \times 10^{-24}$		$6.752 \times 10^{-29}$		$200$
	$1.653 \times 10^{-16}$		$1.220 \times 10^{-19}$		$7.300 \times 10^{-27}$		$3.924 \times 10^{-32}$		$3.596 \times 10^{-26}$
	$1.306 \times 10^{-18}$		$1.017 \times 10^{-19}$		$3.207 \times 10^{-29}$		$8.617 \times 10^{-36}$	60	$2.723 \times 10^{-16}$
	$1.560 \times 10^{-20}$		$4.554 \times 10^{-22}$		$3.610 \times 10^{-24}$		$6.752 \times 10^{-29}$		$400$
	$5.761 \times 10^{-23}$		$1.580 \times 10^{-17}$		$7.300 \times 10^{-27}$		$3.924 \times 10^{-32}$		$1.264 \times 10^{-22}$
	$4.035 \times 10^{-25}$		$8.574 \times 10^{-18}$		$3.207 \times 10^{-29}$		$8.617 \times 10^{-36}$		$200$
	$4.925 \times 10^{-28}$		$1.017 \times 10^{-19}$		$1.831 \times 10^{-32}$		$4.019 \times 10^{-39}$		$3.596 \times 10^{-26}$
	$1.530 \times 10^{-30}$		$4.554 \times 10^{-22}$		$2.765 \times 10^{-35}$		$7.773 \times 10^{-41}$		$400$
	$1.739 \times 10^{-34}$		$1.580 \times 10^{-17}$				$1.524 \times 10^{-44}$		

TABLE S1. Numerical values of the logarithmic negativity contributions from PT symplectic eigenvalues at region separation,  $\tilde{r}$ , presented in Fig. S1.

d = 10						
$\tilde{r}$	$\mathcal{N}_{A B}$	$\mathcal{N}(\sigma_h)_{A B}$	32	$2.762 \times 10^{-5}$	$2.343 \times 10^{-6}$	65
0	$1.214$	$3.575 \times 10^{-1}$	33	$2.211 \times 10^{-5}$	$1.898 \times 10^{-6}$	66
1	$3.915 \times 10^{-1}$	$3.659 \times 10^{-1}$	34	$1.743 \times 10^{-5}$	$1.663 \times 10^{-6}$	67
2	$1.907 \times 10^{-1}$	$3.867 \times 10^{-1}$	35	$1.345 \times 10^{-5}$	$1.553 \times 10^{-6}$	68
3	$1.079 \times 10^{-1}$	$4.306 \times 10^{-1}$	36	$1.010 \times 10^{-5}$	$1.512 \times 10^{-6}$	69
4	$6.725 \times 10^{-2}$	$4.773 \times 10^{-1}$	37	$7.342 \times 10^{-6}$	$1.491 \times 10^{-6}$	70
5	$4.597 \times 10^{-2}$	$1.267 \times 10^{-1}$	38	$5.136 \times 10^{-6}$	$1.437 \times 10^{-6}$	71
6	$3.353 \times 10^{-2}$	$1.406 \times 10^{-1}$	39	$3.454 \times 10^{-6}$	$1.328 \times 10^{-6}$	72
7	$2.546 \times 10^{-2}$	$1.036 \times 10^{-1}$	40	$2.237 \times 10^{-6}$	$1.216 \times 10^{-6}$	73
8	$1.981 \times 10^{-2}$	$3.465 \times 10^{-2}$	41	$1.405 \times 10^{-6}$	$1.194 \times 10^{-6}$	74
9	$1.563 \times 10^{-2}$	$8.211 \times 10^{-3}$	42	$8.728 \times 10^{-7}$	$1.323 \times 10^{-6}$	75
10	$1.243 \times 10^{-2}$	$3.010 \times 10^{-3}$	43	$5.554 \times 10^{-7}$	$1.604 \times 10^{-6}$	76
11	$9.888 \times 10^{-3}$	$1.910 \times 10^{-3}$	44	$3.730 \times 10^{-7}$	$1.977 \times 10^{-6}$	77
12	$7.836 \times 10^{-3}$	$1.381 \times 10^{-3}$	45	$2.655 \times 10^{-7}$	$2.338 \times 10^{-6}$	78
13	$6.154 \times 10^{-3}$	$1.111 \times 10^{-3}$	46	$1.985 \times 10^{-7}$	$2.576 \times 10^{-6}$	79
14	$4.765 \times 10^{-3}$	$9.363 \times 10^{-4}$	47	$1.538 \times 10^{-7}$	$2.609 \times 10^{-6}$	80
15	$3.618 \times 10^{-3}$	$8.215 \times 10^{-4}$	48	$1.223 \times 10^{-7}$	$2.396 \times 10^{-6}$	81
16	$2.680 \times 10^{-3}$	$7.479 \times 10^{-4}$	49	$9.902 \times 10^{-8}$	$1.946 \times 10^{-6}$	82
17	$1.926 \times 10^{-3}$	$7.086 \times 10^{-4}$	50	$8.124 \times 10^{-8}$	$1.320 \times 10^{-6}$	83
18	$1.339 \times 10^{-3}$	$5.565 \times 10^{-4}$	51	$6.723 \times 10^{-8}$	$6.198 \times 10^{-7}$	84
19	$9.043 \times 10^{-4}$	$5.930 \times 10^{-4}$	52	$5.591 \times 10^{-8}$	$4.730 \times 10^{-8}$	85
20	$6.022 \times 10^{-4}$	$6.732 \times 10^{-4}$	53	$4.659 \times 10^{-8}$	$7.074 \times 10^{-9}$	86
21	$4.060 \times 10^{-4}$	$7.785 \times 10^{-4}$	54	$3.878 \times 10^{-8}$	$3.502 \times 10^{-9}$	87
22	$2.835 \times 10^{-4}$	$8.734 \times 10^{-4}$	55	$3.216 \times 10^{-8}$	$2.261 \times 10^{-9}$	88
23	$2.064 \times 10^{-4}$	$9.132 \times 10^{-4}$	56	$2.648 \times 10^{-8}$	$1.668 \times 10^{-9}$	89
24	$1.560 \times 10^{-4}$	$8.631 \times 10^{-4}$	57	$2.157 \times 10^{-8}$	$1.354 \times 10^{-9}$	90
25	$1.212 \times 10^{-4}$	$7.098 \times 10^{-4}$	58	$1.729 \times 10^{-8}$	$1.192 \times 10^{-9}$	91
26	$9.621 \times 10^{-5}$	$4.701 \times 10^{-4}$	59	$1.357 \times 10^{-8}$	$1.133 \times 10^{-9}$	92
27	$7.744 \times 10^{-5}$	$1.997 \times 10^{-4}$	60	$1.033 \times 10^{-8}$	$1.155 \times 10^{-9}$	93
28	$6.289 \times 10^{-5}$	$3.456 \times 10^{-5}$	61	$7.568 \times 10^{-9}$	$1.244 \times 10^{-9}$	94
29	$5.132 \times 10^{-5}$	$1.090 \times 10^{-5}$	62	$5.273 \times 10^{-9}$	$1.374 \times 10^{-9}$	95
30	$4.192 \times 10^{-5}$	$4.814 \times 10^{-6}$	63	$3.479 \times 10^{-9}$	$1.452 \times 10^{-9}$	96
31	$3.414 \times 10^{-5}$	$3.173 \times 10^{-6}$	64	$2.187 \times 10^{-9}$	$1.280 \times 10^{-9}$	97

TABLE S2. Numerical values of region-region logarithmic negativity  $\mathcal{N}_{A|B}(\sigma)$  and the SOE negativity in the halo  $\mathcal{N}_{A|B}(\sigma_h)$  for  $m = 3 \times 10^{-3}/d$  presented in Fig. 2.

$d = 20$													
$\tilde{r}$	$\mathcal{N}_{A B}(\sigma)$	60	$4.480 \times 10^{-5}$	120	$7.296 \times 10^{-9}$	180	$2.103 \times 10^{-12}$	240	$1.870 \times 10^{-16}$	300	$7.682 \times 10^{-21}$	360	$1.813 \times 10^{-25}$
0	1.463	61	$3.764 \times 10^{-5}$	121	$6.571 \times 10^{-9}$	181	$1.815 \times 10^{-12}$	241	$1.456 \times 10^{-16}$	301	$5.902 \times 10^{-21}$	361	$1.434 \times 10^{-25}$
1	$5.438 \times 10^{-1}$	62	$3.149 \times 10^{-5}$	122	$5.921 \times 10^{-9}$	182	$1.553 \times 10^{-12}$	242	$1.129 \times 10^{-16}$	302	$4.645 \times 10^{-21}$	362	$1.171 \times 10^{-25}$
2	$3.187 \times 10^{-1}$	63	$2.628 \times 10^{-5}$	123	$5.337 \times 10^{-9}$	183	$1.315 \times 10^{-12}$	243	$8.731 \times 10^{-17}$	303	$3.746 \times 10^{-21}$	363	$9.786 \times 10^{-26}$
3	$2.209 \times 10^{-1}$	64	$2.191 \times 10^{-5}$	124	$4.808 \times 10^{-9}$	184	$1.103 \times 10^{-12}$	244	$6.756 \times 10^{-17}$	304	$3.088 \times 10^{-21}$	364	$8.336 \times 10^{-26}$
4	$1.648 \times 10^{-1}$	65	$1.828 \times 10^{-5}$	125	$4.328 \times 10^{-9}$	185	$9.152 \times 10^{-13}$	245	$5.253 \times 10^{-17}$	305	$2.595 \times 10^{-21}$	365	$7.207 \times 10^{-26}$
5	$1.283 \times 10^{-1}$	66	$1.530 \times 10^{-5}$	126	$3.891 \times 10^{-9}$	186	$7.518 \times 10^{-13}$	246	$4.126 \times 10^{-17}$	306	$2.215 \times 10^{-21}$	366	$6.305 \times 10^{-26}$
6	$1.032 \times 10^{-1}$	67	$1.288 \times 10^{-5}$	127	$3.491 \times 10^{-9}$	187	$6.119 \times 10^{-13}$	247	$3.288 \times 10^{-17}$	307	$1.916 \times 10^{-21}$	367	$5.570 \times 10^{-26}$
7	$8.490 \times 10^{-2}$	68	$1.090 \times 10^{-5}$	128	$3.126 \times 10^{-9}$	188	$4.940 \times 10^{-13}$	248	$2.664 \times 10^{-17}$	308	$1.675 \times 10^{-21}$	368	$4.960 \times 10^{-26}$
8	$7.111 \times 10^{-2}$	69	$9.288 \times 10^{-6}$	129	$2.791 \times 10^{-9}$	189	$3.961 \times 10^{-13}$	249	$2.197 \times 10^{-17}$	309	$1.478 \times 10^{-21}$	369	$4.446 \times 10^{-26}$
9	$6.034 \times 10^{-2}$	70	$7.972 \times 10^{-6}$	130	$2.483 \times 10^{-9}$	190	$3.159 \times 10^{-13}$	250	$1.841 \times 10^{-17}$	310	$1.314 \times 10^{-21}$	370	$4.007 \times 10^{-26}$
10	$5.171 \times 10^{-2}$	71	$6.889 \times 10^{-6}$	131	$2.201 \times 10^{-9}$	191	$2.509 \times 10^{-13}$	251	$1.565 \times 10^{-17}$	311	$1.175 \times 10^{-21}$	371	$3.628 \times 10^{-26}$
11	$4.466 \times 10^{-2}$	72	$5.992 \times 10^{-6}$	132	$1.941 \times 10^{-9}$	192	$1.988 \times 10^{-13}$	252	$1.347 \times 10^{-17}$	312	$1.057 \times 10^{-21}$	372	$3.297 \times 10^{-26}$
12	$3.881 \times 10^{-2}$	73	$5.242 \times 10^{-6}$	133	$1.703 \times 10^{-9}$	193	$1.576 \times 10^{-13}$	253	$1.172 \times 10^{-17}$	313	$9.546 \times 10^{-22}$	373	$3.007 \times 10^{-26}$
13	$3.388 \times 10^{-2}$	74	$4.610 \times 10^{-6}$	134	$1.484 \times 10^{-9}$	194	$1.254 \times 10^{-13}$	254	$1.029 \times 10^{-17}$	314	$8.656 \times 10^{-22}$	374	$2.750 \times 10^{-26}$
14	$2.966 \times 10^{-2}$	75	$4.072 \times 10^{-6}$	135	$1.285 \times 10^{-9}$	195	$1.005 \times 10^{-13}$	255	$9.099 \times 10^{-18}$	315	$7.873 \times 10^{-22}$	375	$2.520 \times 10^{-26}$
15	$2.602 \times 10^{-2}$	76	$3.610 \times 10^{-6}$	136	$1.104 \times 10^{-9}$	196	$8.138 \times 10^{-14}$	256	$8.101 \times 10^{-18}$	316	$7.181 \times 10^{-22}$	376	$2.314 \times 10^{-26}$
16	$2.285 \times 10^{-2}$	77	$3.211 \times 10^{-6}$	137	$9.414 \times 10^{-10}$	197	$6.672 \times 10^{-14}$	257	$7.253 \times 10^{-18}$	317	$6.563 \times 10^{-22}$	377	$2.128 \times 10^{-26}$
17	$2.006 \times 10^{-2}$	78	$2.863 \times 10^{-6}$	138	$7.956 \times 10^{-10}$	198	$5.543 \times 10^{-14}$	258	$6.523 \times 10^{-18}$	318	$6.009 \times 10^{-22}$	382	$1.418 \times 10^{-26}$
18	$1.759 \times 10^{-2}$	79	$2.557 \times 10^{-6}$	139	$6.665 \times 10^{-10}$	199	$4.665 \times 10^{-14}$	259	$5.890 \times 10^{-18}$	319	$5.510 \times 10^{-22}$	388	$1.960 \times 10^{-26}$
19	$1.541 \times 10^{-2}$	80	$2.288 \times 10^{-6}$	140	$5.537 \times 10^{-10}$	200	$3.975 \times 10^{-14}$	260	$5.336 \times 10^{-18}$	320	$5.058 \times 10^{-22}$	379	$1.806 \times 10^{-26}$
20	$1.346 \times 10^{-2}$	81	$2.048 \times 10^{-6}$	141	$4.563 \times 10^{-10}$	201	$3.424 \times 10^{-14}$	261	$4.847 \times 10^{-18}$	321	$4.646 \times 10^{-22}$	380	$1.666 \times 10^{-26}$
21	$1.173 \times 10^{-2}$	82	$1.834 \times 10^{-6}$	142	$3.734 \times 10^{-10}$	202	$2.978 \times 10^{-14}$	262	$4.413 \times 10^{-18}$	322	$4.270 \times 10^{-22}$	381	$1.537 \times 10^{-26}$
22	$1.018 \times 10^{-2}$	83	$1.642 \times 10^{-6}$	143	$3.038 \times 10^{-10}$	203	$2.611 \times 10^{-14}$	263	$4.025 \times 10^{-18}$	323	$3.925 \times 10^{-22}$	382	$1.418 \times 10^{-26}$
23	$8.805 \times 10^{-3}$	84	$1.469 \times 10^{-6}$	144	$2.461 \times 10^{-10}$	204	$2.306 \times 10^{-14}$	264	$3.676 \times 10^{-18}$	324	$3.607 \times 10^{-22}$	383	$1.308 \times 10^{-26}$
24	$7.579 \times 10^{-3}$	85	$1.313 \times 10^{-6}$	145	$1.990 \times 10^{-10}$	205	$2.049 \times 10^{-14}$	265	$3.361 \times 10^{-18}$	325	$3.314 \times 10^{-22}$	384	$1.207 \times 10^{-26}$
25	$6.493 \times 10^{-3}$	86	$1.171 \times 10^{-6}$	146	$1.608 \times 10^{-10}$	206	$1.830 \times 10^{-14}$	266	$3.075 \times 10^{-18}$	326	$3.042 \times 10^{-22}$	385	$1.112 \times 10^{-26}$
26	$5.536 \times 10^{-3}$	87	$1.043 \times 10^{-6}$	147	$1.304 \times 10^{-10}$	207	$1.642 \times 10^{-14}$	267	$2.814 \times 10^{-18}$	327	$2.790 \times 10^{-22}$	386	$1.024 \times 10^{-26}$
27	$4.700 \times 10^{-3}$	88	$9.253 \times 10^{-7}$	148	$1.063 \times 10^{-10}$	208	$1.479 \times 10^{-14}$	268	$2.576 \times 10^{-18}$	328	$2.555 \times 10^{-22}$	387	$9.416 \times 10^{-27}$
28	$3.975 \times 10^{-3}$	89	$8.185 \times 10^{-7}$	149	$8.742 \times 10^{-11}$	209	$1.335 \times 10^{-14}$	269	$2.357 \times 10^{-18}$	329	$2.336 \times 10^{-22}$	388	$8.645 \times 10^{-27}$
29	$3.353 \times 10^{-3}$	90	$7.210 \times 10^{-7}$	150	$7.258 \times 10^{-11}$	210	$1.209 \times 10^{-14}$	270	$2.155 \times 10^{-18}$	330	$2.132 \times 10^{-22}$	389	$7.922 \times 10^{-27}$
30	$2.826 \times 10^{-3}$	91	$6.323 \times 10^{-7}$	151	$6.090 \times 10^{-11}$	211	$1.097 \times 10^{-14}$	271	$1.969 \times 10^{-18}$	331	$1.940 \times 10^{-22}$	390	$7.243 \times 10^{-27}$
31	$2.383 \times 10^{-3}$	92	$5.515 \times 10^{-7}$	152	$5.164 \times 10^{-11}$	212	$9.972 \times 10^{-15}$	272	$1.797 \times 10^{-18}$	332	$1.760 \times 10^{-22}$	391	$6.603 \times 10^{-27}$
32	$2.014 \times 10^{-3}$	93	$4.783 \times 10^{-7}$	153	$4.424 \times 10^{-11}$	213	$9.074 \times 10^{-15}$	273	$1.637 \times 10^{-18}$	333	$1.591 \times 10^{-22}$	392	$5.999 \times 10^{-27}$
33	$1.710 \times 10^{-3}$	94	$4.121 \times 10^{-7}$	154	$3.825 \times 10^{-11}$	214	$8.263 \times 10^{-15}$	274	$1.488 \times 10^{-18}$	334	$1.432 \times 10^{-22}$	393	$5.430 \times 10^{-27}$
34	$1.458 \times 10^{-3}$	95	$3.526 \times 10^{-7}$	155	$3.334 \times 10^{-11}$	215	$7.527 \times 10^{-15}$	275	$1.349 \times 10^{-18}$	335	$1.282 \times 10^{-22}$	394	$4.891 \times 10^{-27}$
35	$1.251 \times 10^{-3}$	96	$2.996 \times 10^{-7}$	156	$2.927 \times 10^{-11}$	216	$6.858 \times 10^{-15}$	276	$1.219 \times 10^{-18}$	336	$1.141 \times 10^{-22}$	395	$4.380 \times 10^{-27}$
36	$1.079 \times 10^{-3}$	97	$2.527 \times 10^{-7}$	157	$2.586 \times 10^{-11}$	217	$6.246 \times 10^{-15}$	277	$1.097 \times 10^{-18}$	337	$1.008 \times 10^{-22}$	396	$3.897 \times 10^{-27}$
37	$9.367 \times 10^{-4}$	98	$2.116 \times 10^{-7}$	158	$2.297 \times 10^{-11}$	218	$5.685 \times 10^{-15}$	278	$9.839 \times 10^{-19}$	338	$8.823 \times 10^{-23}$	397	$3.438 \times 10^{-27}$
38	$8.170 \times 10^{-4}$	99	$1.761 \times 10^{-7}$	159	$2.050 \times 10^{-11}$	219	$5.169 \times 10^{-15}$	279	$8.774 \times 10^{-19}$	339	$7.644 \times 10^{-23}$	398	$3.002 \times 10^{-27}$
39	$7.160 \times 10^{-4}$	100	$1.457 \times 10^{-7}$	160	$1.836 \times 10^{-11}$	220	$4.693 \times 10^{-15}$	280	$7.777 \times 10^{-19}$	340	$6.536 \times 10^{-23}$	399	$2.589 \times 10^{-27}$
40	$6.299 \times 10^{-4}$	101	$1.201 \times 10^{-7}$	161	$1.650 \times 10^{-11}$	221	$4.252 \times 10^{-15}$	281	$6.844 \times 10^{-19}$	341	$5.503 \times 10^{-23}$	400	$2.196 \times 10^{-27}$
41	$5.561 \times 10^{-4}$	102	$9.870 \times 10^{-8}$	162	$1.487 \times 10^{-11}$	222	$3.844 \times 10^{-15}$	282	$5.971 \times 10^{-19}$	342	$4.545 \times 10^{-23}$	401	$1.825 \times 10^{-27}$
42	$4.922 \times 10^{-4}$	103	$8.113 \times 10^{-8}$	163	$1.342 \times 10^{-11}$	223	$3.466 \times 10^{-15}$	283	$5.157 \times 10^{-19}$	343	$3.670 \times 10^{-23}$	402	$1.475 \times 10^{-27}$
43	$4.366 \times 10^{-4}$	104	$6.683 \times 10^{-8}$	164	$1.214 \times 10^{-11}$	224	$3.114 \times 10^{-15}$	284	$4.402 \times 10^{-19}$	344	$2.889 \times 10^{-23}$	403	$1.148 \times 10^{-27}$
44	$3.878 \times 10^{-4}$	105	$5.531 \times 10^{-8}$	165	$1.099 \times 10^{-11}$	225	$2.786 \times 10^{-15}$	285	$3.706 \times 10^{-19}$	345	$2.214 \times 10^{-23}$	404	$8.493 \times 10^{-28}$
45	$3.447 \times 10^{-4}$	106	$4.608 \times 10^{-8}$	166	$9.959 \times 10^{-12}$	226	$2.481 \times 10^{-15}$	286	$3.073 \times 10^{-19}$	346	$1.659 \times 10^{-23}$	405	$5.878 \times 10^{-28}$
46	$3.065 \times 10^{-4}$	107	$3.869 \times 10^{-8}$	167	$9.027 \times 10^{-12}$	227	$2.197 \times 10^{-15}$	287	$2.506 \times 10^{-19}$	347	$1.225 \times 10^{-23}$	406	$3.797 \times 10^{-28}$
47	$2.725 \times 10^{-4}$	108	$3.277 \times 10^{-8}$	168	$8.181 \times 10^{-12}$	228	$1.932 \times 10^{-15}$	288	$2.009 \times 10^{-19}$	348	$9.012 \times 10^{-24}$	407	$2.373 \times 10^{-28}$
48	$2.420 \times 10^{-4}$	109	$2.799 \times 10^{-8}$	169	$7.411 \times 10^{-12}$	229	$1.687 \times 10^{-15}$	289	$1.585 \times 10^{-19}$	349	$6.647 \times 10^{-24}$	408	$1.516 \times 10^{-28}$
49	$2.147 \times 10^{-4}$	110	$2.411 \times 10^{-8}$	170	$6.707 \times 10^{-12}$	230	$1.460 \times 10^{-15}$	290	$1.235 \times 10^{-19}$	350	$4.925 \times 10^{-24}$	409	$1.014 \times 10^{-28}$
50	$1.901 \times 10^{-4}$	111	$2.093 \times 10^{-8}$	171	$6.$								

$d = 20$													
$\bar{r}$	$\mathcal{N}(\sigma_h)_{A B}$	60	$2.262 \times 10^{-5}$	120	$1.049 \times 10^{-8}$	180	$2.611 \times 10^{-13}$	240	$1.351 \times 10^{-16}$	300	$1.932 \times 10^{-20}$	360	$1.939 \times 10^{-24}$
0	$4.818 \times 10^{-1}$	61	$2.290 \times 10^{-5}$	121	$3.449 \times 10^{-9}$	181	$2.643 \times 10^{-13}$	241	$1.139 \times 10^{-16}$	301	$2.287 \times 10^{-20}$	361	$2.537 \times 10^{-24}$
1	$4.862 \times 10^{-1}$	62	$2.334 \times 10^{-5}$	122	$1.625 \times 10^{-9}$	182	$2.697 \times 10^{-13}$	242	$1.006 \times 10^{-16}$	302	$2.734 \times 10^{-20}$	362	$3.275 \times 10^{-24}$
2	$5.027 \times 10^{-1}$	63	$2.395 \times 10^{-5}$	123	$1.005 \times 10^{-9}$	183	$2.762 \times 10^{-13}$	243	$9.483 \times 10^{-17}$	303	$3.255 \times 10^{-20}$	363	$4.177 \times 10^{-24}$
3	$5.444 \times 10^{-1}$	64	$2.470 \times 10^{-5}$	124	$7.117 \times 10^{-10}$	184	$2.822 \times 10^{-13}$	244	$9.515 \times 10^{-17}$	304	$3.834 \times 10^{-20}$	364	$5.274 \times 10^{-24}$
4	$5.852 \times 10^{-1}$	65	$2.555 \times 10^{-5}$	125	$5.454 \times 10^{-10}$	185	$2.859 \times 10^{-13}$	245	$1.005 \times 10^{-16}$	305	$4.446 \times 10^{-20}$	365	$6.595 \times 10^{-24}$
5	$6.224 \times 10^{-1}$	66	$2.644 \times 10^{-5}$	126	$4.412 \times 10^{-10}$	186	$2.853 \times 10^{-13}$	246	$1.101 \times 10^{-16}$	306	$5.067 \times 10^{-20}$	366	$8.162 \times 10^{-24}$
6	$6.562 \times 10^{-1}$	67	$2.726 \times 10^{-5}$	127	$3.718 \times 10^{-10}$	187	$2.787 \times 10^{-13}$	247	$1.232 \times 10^{-16}$	307	$5.664 \times 10^{-20}$	370	$1.647 \times 10^{-23}$
7	$1.953 \times 10^{-1}$	68	$2.790 \times 10^{-5}$	128	$3.239 \times 10^{-10}$	188	$2.661 \times 10^{-13}$	248	$1.389 \times 10^{-16}$	308	$6.205 \times 10^{-20}$	371	$9.978 \times 10^{-24}$
8	$1.733 \times 10^{-1}$	69	$2.823 \times 10^{-5}$	129	$2.903 \times 10^{-10}$	189	$2.496 \times 10^{-13}$	249	$1.562 \times 10^{-16}$	309	$6.655 \times 10^{-20}$	368	$1.201 \times 10^{-23}$
9	$1.522 \times 10^{-1}$	70	$2.815 \times 10^{-5}$	130	$2.667 \times 10^{-10}$	190	$2.329 \times 10^{-13}$	250	$1.739 \times 10^{-16}$	310	$6.980 \times 10^{-20}$	369	$1.421 \times 10^{-23}$
10	$1.250 \times 10^{-1}$	71	$2.759 \times 10^{-5}$	131	$2.504 \times 10^{-10}$	191	$2.197 \times 10^{-13}$	251	$1.910 \times 10^{-16}$	311	$7.155 \times 10^{-20}$	370	$1.647 \times 10^{-23}$
11	$4.682 \times 10^{-2}$	72	$2.640 \times 10^{-5}$	132	$2.396 \times 10^{-10}$	192	$2.126 \times 10^{-13}$	252	$2.062 \times 10^{-16}$	312	$7.161 \times 10^{-20}$	371	$1.869 \times 10^{-23}$
12	$2.720 \times 10^{-2}$	73	$2.463 \times 10^{-5}$	133	$2.330 \times 10^{-10}$	193	$2.123 \times 10^{-13}$	253	$2.185 \times 10^{-16}$	313	$6.990 \times 10^{-20}$	372	$2.074 \times 10^{-23}$
13	$1.697 \times 10^{-2}$	74	$2.229 \times 10^{-5}$	134	$2.296 \times 10^{-10}$	194	$2.190 \times 10^{-13}$	254	$2.268 \times 10^{-16}$	314	$6.646 \times 10^{-20}$	373	$2.251 \times 10^{-23}$
14	$1.144 \times 10^{-2}$	75	$1.937 \times 10^{-5}$	135	$2.286 \times 10^{-10}$	195	$2.318 \times 10^{-13}$	255	$2.305 \times 10^{-16}$	315	$6.146 \times 10^{-20}$	374	$2.390 \times 10^{-23}$
15	$8.260 \times 10^{-3}$	76	$1.598 \times 10^{-5}$	136	$2.291 \times 10^{-10}$	196	$2.495 \times 10^{-13}$	256	$2.290 \times 10^{-16}$	316	$5.516 \times 10^{-20}$	375	$2.480 \times 10^{-23}$
16	$6.366 \times 10^{-3}$	77	$1.225 \times 10^{-5}$	137	$2.304 \times 10^{-10}$	197	$2.706 \times 10^{-13}$	257	$2.221 \times 10^{-16}$	317	$4.791 \times 10^{-20}$	376	$2.516 \times 10^{-23}$
17	$5.167 \times 10^{-3}$	78	$8.371 \times 10^{-6}$	138	$2.314 \times 10^{-10}$	198	$2.933 \times 10^{-13}$	258	$2.099 \times 10^{-16}$	318	$4.011 \times 10^{-20}$	377	$2.491 \times 10^{-23}$
18	$4.262 \times 10^{-3}$	79	$4.698 \times 10^{-6}$	139	$2.317 \times 10^{-10}$	199	$3.156 \times 10^{-13}$	259	$1.930 \times 10^{-16}$	319	$3.215 \times 10^{-20}$	378	$2.402 \times 10^{-23}$
19	$3.578 \times 10^{-3}$	80	$2.065 \times 10^{-6}$	140	$2.309 \times 10^{-10}$	200	$3.356 \times 10^{-13}$	260	$1.720 \times 10^{-16}$	320	$2.436 \times 10^{-20}$	379	$2.250 \times 10^{-23}$
20	$3.097 \times 10^{-3}$	81	$9.659 \times 10^{-7}$	141	$2.285 \times 10^{-10}$	201	$3.515 \times 10^{-13}$	261	$1.480 \times 10^{-16}$	321	$1.700 \times 10^{-20}$	380	$2.037 \times 10^{-23}$
21	$2.783 \times 10^{-3}$	82	$5.701 \times 10^{-7}$	142	$2.091 \times 10^{-10}$	202	$3.616 \times 10^{-13}$	262	$1.220 \times 10^{-16}$	322	$1.024 \times 10^{-20}$	381	$1.773 \times 10^{-23}$
22	$2.541 \times 10^{-3}$	83	$3.910 \times 10^{-7}$	143	$2.060 \times 10^{-10}$	203	$3.648 \times 10^{-13}$	263	$9.527 \times 10^{-17}$	323	$4.186 \times 10^{-21}$	382	$1.475 \times 10^{-23}$
23	$2.414 \times 10^{-3}$	84	$2.933 \times 10^{-7}$	144	$2.040 \times 10^{-10}$	204	$3.602 \times 10^{-13}$	264	$6.880 \times 10^{-17}$	324	$1.796 \times 10^{-22}$	383	$1.166 \times 10^{-23}$
24	$2.339 \times 10^{-3}$	85	$1.883 \times 10^{-7}$	145	$2.044 \times 10^{-10}$	205	$3.474 \times 10^{-13}$	265	$4.349 \times 10^{-17}$	325	$3.953 \times 10^{-23}$	384	$8.733 \times 10^{-24}$
25	$2.303 \times 10^{-3}$	86	$1.594 \times 10^{-7}$	146	$2.080 \times 10^{-10}$	206	$3.266 \times 10^{-13}$	266	$2.008 \times 10^{-17}$	326	$2.149 \times 10^{-23}$	385	$6.184 \times 10^{-24}$
26	$2.315 \times 10^{-3}$	87	$1.392 \times 10^{-7}$	147	$2.151 \times 10^{-10}$	207	$2.984 \times 10^{-13}$	267	$2.482 \times 10^{-18}$	327	$1.456 \times 10^{-23}$	386	$4.125 \times 10^{-24}$
27	$2.356 \times 10^{-3}$	88	$1.249 \times 10^{-7}$	148	$2.254 \times 10^{-10}$	208	$2.638 \times 10^{-13}$	268	$4.809 \times 10^{-19}$	328	$1.094 \times 10^{-23}$	387	$2.536 \times 10^{-24}$
28	$2.416 \times 10^{-3}$	89	$1.148 \times 10^{-7}$	149	$2.382 \times 10^{-10}$	209	$2.242 \times 10^{-13}$	269	$2.475 \times 10^{-19}$	329	$8.744 \times 10^{-24}$	388	$1.337 \times 10^{-24}$
29	$2.488 \times 10^{-3}$	90	$1.075 \times 10^{-7}$	150	$2.522 \times 10^{-10}$	210	$1.813 \times 10^{-13}$	270	$1.628 \times 10^{-19}$	330	$7.301 \times 10^{-24}$	389	$4.339 \times 10^{-25}$
30	$2.569 \times 10^{-3}$	91	$1.025 \times 10^{-7}$	151	$2.660 \times 10^{-10}$	211	$1.369 \times 10^{-13}$	271	$1.198 \times 10^{-19}$	331	$6.305 \times 10^{-24}$	390	$2.655 \times 10^{-27}$
31	$2.649 \times 10^{-3}$	92	$9.904 \times 10^{-8}$	152	$2.782 \times 10^{-10}$	212	$9.274 \times 10^{-14}$	272	$9.413 \times 10^{-20}$	332	$5.602 \times 10^{-24}$	391	$7.780 \times 10^{-28}$
32	$2.720 \times 10^{-3}$	93	$9.684 \times 10^{-8}$	153	$2.873 \times 10^{-10}$	213	$5.057 \times 10^{-14}$	273	$7.742 \times 10^{-20}$	333	$5.105 \times 10^{-24}$	392	$4.614 \times 10^{-28}$
33	$2.768 \times 10^{-3}$	94	$9.553 \times 10^{-8}$	154	$2.919 \times 10^{-10}$	214	$1.436 \times 10^{-14}$	274	$6.596 \times 10^{-20}$	334	$4.763 \times 10^{-24}$	393	$3.325 \times 10^{-28}$
34	$2.782 \times 10^{-3}$	95	$9.476 \times 10^{-8}$	155	$2.912 \times 10^{-10}$	215	$2.509 \times 10^{-15}$	275	$5.787 \times 10^{-20}$	335	$4.548 \times 10^{-24}$	394	$2.637 \times 10^{-28}$
35	$2.746 \times 10^{-3}$	96	$9.426 \times 10^{-8}$	156	$2.844 \times 10^{-10}$	216	$1.125 \times 10^{-15}$	276	$5.213 \times 10^{-20}$	336	$4.441 \times 10^{-24}$	395	$2.220 \times 10^{-28}$
36	$2.631 \times 10^{-3}$	97	$9.390 \times 10^{-8}$	157	$2.713 \times 10^{-10}$	217	$6.987 \times 10^{-16}$	277	$4.811 \times 10^{-20}$	337	$4.437 \times 10^{-24}$	396	$1.950 \times 10^{-28}$
37	$2.483 \times 10^{-3}$	98	$9.382 \times 10^{-8}$	158	$2.519 \times 10^{-10}$	218	$4.971 \times 10^{-16}$	278	$4.545 \times 10^{-20}$	338	$4.534 \times 10^{-24}$	397	$1.773 \times 10^{-28}$
38	$2.255 \times 10^{-3}$	99	$9.411 \times 10^{-8}$	159	$2.267 \times 10^{-10}$	219	$3.817 \times 10^{-16}$	279	$4.390 \times 10^{-20}$	339	$4.742 \times 10^{-24}$	398	$1.660 \times 10^{-28}$
39	$1.947 \times 10^{-3}$	100	$9.479 \times 10^{-8}$	160	$1.965 \times 10^{-10}$	220	$3.084 \times 10^{-16}$	280	$4.335 \times 10^{-20}$	340	$5.075 \times 10^{-24}$	399	$1.598 \times 10^{-28}$
40	$1.571 \times 10^{-3}$	101	$9.599 \times 10^{-8}$	161	$1.624 \times 10^{-10}$	221	$2.590 \times 10^{-16}$	281	$4.372 \times 10^{-20}$	341	$5.560 \times 10^{-24}$	400	$1.583 \times 10^{-28}$
41	$1.152 \times 10^{-3}$	102	$9.790 \times 10^{-8}$	162	$1.258 \times 10^{-10}$	222	$2.244 \times 10^{-16}$	282	$4.500 \times 10^{-20}$	342	$6.229 \times 10^{-24}$	401	$1.618 \times 10^{-28}$
42	$7.358 \times 10^{-4}$	103	$1.006 \times 10^{-7}$	163	$8.813 \times 10^{-11}$	223	$2.000 \times 10^{-16}$	283	$4.721 \times 10^{-20}$	343	$7.124 \times 10^{-24}$	402	$1.714 \times 10^{-28}$
43	$4.036 \times 10^{-4}$	104	$1.042 \times 10^{-7}$	164	$5.128 \times 10^{-11}$	224	$1.827 \times 10^{-16}$	284	$5.041 \times 10^{-20}$	344	$8.275 \times 10^{-24}$	403	$1.902 \times 10^{-28}$
44	$2.179 \times 10^{-4}$	105	$1.084 \times 10^{-7}$	165	$1.900 \times 10^{-11}$	225	$1.708 \times 10^{-16}$	285	$5.462 \times 10^{-20}$	345	$9.658 \times 10^{-24}$	404	$2.237 \times 10^{-28}$
45	$1.333 \times 10^{-4}$	106	$1.129 \times 10^{-7}$	166	$4.610 \times 10^{-12}$	226	$1.633 \times 10^{-16}$	286	$5.982 \times 10^{-20}$	346	$1.111 \times 10^{-23}$	405	$2.836 \times 10^{-28}$
46	$9.177 \times 10^{-5}$	107	$1.171 \times 10^{-7}$	167	$2.033 \times 10^{-12}$	227	$1.594 \times 10^{-16}$	287	$6.576 \times 10^{-20}$	347	$1.226 \times 10^{-23}$	406	$3.892 \times 10^{-28}$
47	$6.856 \times 10^{-5}$	108	$1.205 \times 10^{-7}$	168	$1.239 \times 10^{-12}$	228	$1.586 \times 10^{-16}$	288	$7.180 \times 10^{-20}$	348	$1.252 \times 10^{-23}$	407	$5.582 \times 10^{-28}$
48	$5.454 \times 10^{-5}$	109	$1.226 \times 10^{-7}$	169	$8.700 \times 10^{-13}$	229	$1.606 \times 10^{-16}$	289	$7.671 \times 10^{-20}$	349	$1.131 \times 10^{-23}$	408	$7.878 \times 10^{-28}$
49	$4.523 \times 10^{-5}$	110	$1.227 \times 10^{-7}$	170	$6.615 \times 10^{-13}$	230	$1.652 \times 10^{-16}$	290	$7.855 \times 10^{-20}$	350	$8.285 \times 10^{-24}$	409	$1.060 \times 10^{-27}$
50	$3.871 \times 10^{-5}$	111	$1.206 \times 10^{-7}$	171	$5.304 \times 10^{-13}$	23							